FFI RAPPORT

OBSERVABILITY AT HF DIRECTION FINDING SITES OF SCATTERING FROM WIND FARMS – Measurements at Smøla 2006

OTNES Roald, HJELMSTAD Jens

FFI/RAPPORT-2006/02701

OBSERVABILITY AT HF DIRECTION FINDING SITES OF SCATTERING FROM WIND FARMS – Measurements at Smøla 2006

OTNES Roald, HJELMSTAD Jens

FFI/RAPPORT-2006/02701

FORSVARETS FORSKNINGSINSTITUTT
Norwegian Defence Research Establishment
P O Box 25, NO-2027 Kjeller, Norway

FORSVARETS FORSKNINGSINSTITUTT(FFI)
Norwegian Defence Research Establishment

P O BOX 25
NO-2027 KJELLER, NORWAY

UNCLASSIFIED

SECURITY CLASSIFICATION OF THIS PAGE
(when data entered)

REPORT DOCUMENTATION PAGE

1) PUBL/REPORT NUMBER	2) SECURITY CLASSIFICATION	3) NUMBER OF PAGES
FFI/RAPPORT-2006/02701	UNCLASSIFIED	57
1a) PROJECT REFERENCE	**2a) DECLASSIFICATION/DOWNGRADING SCHEDULE**	
FFI-II/1013/912	-	

4) TITLE

OBSERVABILITY AT HF DIRECTION FINDING SITES OF SCATTERING FROM WIND FARMS – Measurements at Smøla 2006

5) NAMES OF AUTHOR(S) IN FULL (surname first)

OTNES Roald, HJELMSTAD Jens

6) DISTRIBUTION STATEMENT

Approved for public release. Distribution unlimited. (Offentlig tilgjengelig)

7) INDEXING TERMS

IN ENGLISH	IN NORWEGIAN
a) Wind turbine	a) Vindmølle
b) Wind farm	b) Vindkraftverk
c) High frequency radio	c) HF-radio
d) Direction finding	d) Peiling
e) Scattering	e) Spredning

THESAURUS REFERENCE:

8) ABSTRACT

This report studies, on a general basis, whether wind farms may decrease the accuracy of direction finding systems in the HF (high frequency, 2-30 MHz) band, due to scattering from the wind turbine towers or blades. Theoretical considerations are accompanied by a three-day measurement campaign at Smøla, a large wind farm with 68 wind turbines installed. The measurements provide evidence that the wind farm causes direction finding errors when it is between transmitter and receiver, but also shows errors of similar level at other angles, which are more likely attributed to topographic features than to the wind farm. Additionally, the measurements revealed an unexpected effect of much larger errors at certain positions, which seem to be modulated by blade rotation. A more comprehensive measurement campaign would be required to fully understand the observed effects.

9) DATE	AUTHORIZED BY	POSITION
2005-09-07	This page only Vidar S Andersen	Director

ISBN 82-464-1022-9

FFI-B-22-1982

UNCLASSIFIED

SECURITY CLASSIFICATION OF THIS PAGE
(when data entered)

CONTENTS

page

OBSERVABILITY AT HF DIRECTION FINDING SITES OF SCATTERING FROM WIND FARMS

Measurements at Smøla 2006

1 EXECUTIVE SUMMARY

A large number of onshore and offshore wind farms are currently being planned and commissioned. Many countries have well established procedures for assessing the impact of wind farms on society and natural environments. Some aspects regarding their influence on direction finding and communication systems have however not been studied extensively and guidelines are not in place.

This report considers the influence by scattering effects of wind farms on HF radio communication and direction finding systems. Theoretical studies have been performed, as well as a measurement campaign at the Smøla wind farm (with 68 wind turbines installed). The transmitter was located on a boat in order to traverse different transmitter positions, and the receiver was a two-element interferometer with high-quality measurement equipment. The measurement frequencies were in the range 2-10 MHz where the scattering effects by theoretical considerations are expected to be maximal.

When the transmitter-receiver path passes over or near the wind farm, the experiments have uncovered larger than expected phase fluctuations for certain locations. When the transmitter-receiver path is outside the wind farm (2-15 degrees away from wind farm boundary) no effects likely to be attributed to the wind farm were observed in the experiments.

The overall conclusion of this study is that specific care and consideration should be taken when wind farms are positioned near the line of sight of HF communication and direction finding services utilizing potential ground wave paths (up 50 km range over land and 500 km over sea). To quantify and confirm the observed effects, further measurements would be required. For non-line of sight (sky wave) arrangements influences are expected to be weaker, but further studies would be required in order to identify possible sky wave effects, in particular for transmitters behind the wind farm.

2 INTRODUCTION

This report describes a joint study between Roald Otnes of FFI and Jens Hjelmstad of NTNU. Otnes' participation in the study is part of project 1013 "Vindkraft" at FFI, while Hjelmstad's participation in the study is sponsored by Statkraft AS.

A large number of onshore and offshore wind farms are currently being planned and commissioned. Many countries have well established procedures for assessing the impact of wind farms on society and natural environments. Some aspects regarding their influence on direction finding and communication systems have however not been studied extensively and

guidelines are not in place.

This report considers specifically the influence of wind farms on HF radio communication and direction finding systems. Simple theoretical models suggest that at these frequencies the wind turbines have their worst case influence on the propagation and scattering of electromagnetic waves, due to the resonant conditions that exist between the wavelength of the radiation and the physical size of the wind turbines. It was therefore reasoned that specific studies should be carried out on these frequencies as the effects are most pronounced and most easily measured, and experimental findings could be extrapolated to other less affected frequency domains.

As a consequence of this, a specific study has been performed of available literature and experimental data, and an updated and cross-referenced model of scattering has been established. Updated values of propagation and scattering parameters need to be generated with the basis of these findings.

The study has been performed in a short time frame, April-August 2006. It has encompassed theoretical elaborations, planning and execution of a measurement campaign, as well as processing and interpretation of measurement results.

The outline of the report is as follows. Sec. 3 presents theoretical considerations, which were mostly written before the measurement campaign. Sec. 4 presents the measurement campaign, including description of measurement setup, presentation of results, summarizing discussion, and lessons learned. Finally, conclusions are drawn in Sec. 5.

3 THEORETICAL BACKGROUND

Previously published works on scattering of HF radio waves (2-30 MHz) from wind farms are very sparse. In the 1970’s, Sengupta published numerous papers and reports (see e.g. [8]) on scattering effects from wind turbines on TV signals, but these are from 50 MHz and upwards. The only public study we have found of relevance to HF scattering from wind farms is a report from FOI in Sweden [1]. The Swedish study presents numerical simulations of scattering from a single wind turbine, and presents a method to model scattering from a complete wind farm by coherent addition of the scattering from each wind turbine (ignoring effects such as multiple scattering or mutual coupling between wind farms). The theoretical elaborations presented in the present chapter are heavily based on [1].

3.1 Problem definition

Consider the model depicted in Fig. 3.1, where an incoming electromagnetic wave carrying a signal of interest from a remote transmitter location is incident on the receiver site as well as at the wind farm. Scattering effects will cause the signal to be reradiated from the wind farm in all directions, such that a delayed version of the signal will appear to be incident from the direction of the wind farm.

For simple analysis, we make the following assumptions:

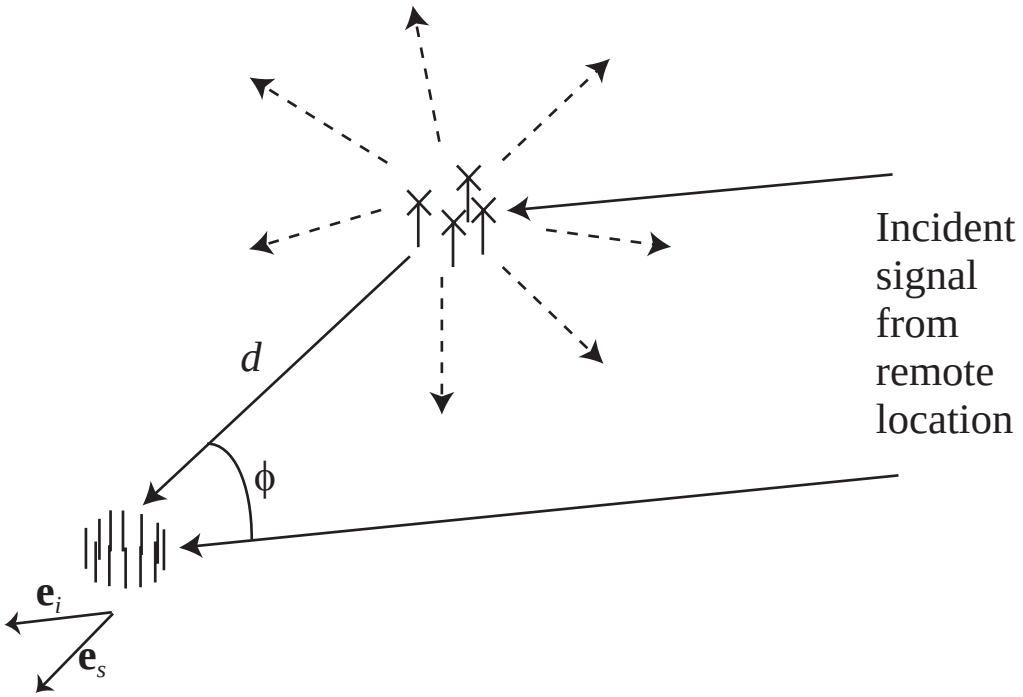

Figure 3.1 Scattering model

1. The transmitter is so far away that the incident signal is equal at the receiver site and at the wind farm (except for a time delay difference τ_d). In particular, the directions of incidence and the path losses are assumed equal for both paths from the remote transmitter.

2. The distance between receiver and wind farm is sufficiently large that the scattered signal appears to come from a point source, and that wavefront curvature over the size of the receiver antenna can be neglected

3. Wavefront curvature of the incident signal from remote transmitter is negligible at the wind farm as well as at the receiver station

4. Other scattering effects are not considered for the present discussion. I.e., the incoming signal in the absence of wind turbines is assumed to have a single angle of incidence and not suffer multipath effects.

5. The formulas describing incident electromagnetic waves describe the electrical field in the absence of local perturbations caused by the antenna structures or wind turbines.

6. The following theoretical discussion only considers static scattering effects. Shadowing, radiation (EMC noise), and modulated scattering effects due to blade rotation are not considered. In reality, modulation by blade rotation is however possible: Even though the blades are often epoxy material, they will in general have metal lightning conductors along their side such that they may contribute to scattering of electromagnetic waves.

The electrical field associated with an incoming electromagnetic signal at the receiver site, in

the absence of wind turbines and other scattering effects, can be written

$$\mathbf{E}_i(t,\mathbf{r}) = \Re\left\{E_i(t)\mathbf{p}_i e^{j(\omega t - k\mathbf{e}_i\cdot\mathbf{r})}\right\} \tag{3.1}$$

Here, $\omega = 2\pi f$ is the center frequency, $k = 2\pi/\lambda$ is the wave number, and $\mathbf{e}_i$ is a unit vector pointing in the direction of propagation such that $\mathbf{k}_i = k\mathbf{e}_i$ is the wave number vector. $E_i(t)$ is the complex baseband equivalent of the information-carrying signal. $\mathbf{r}$ is the position vector referred to the origin of the direction finding system, and $\mathbf{p}_i$ is a unit vector defining the polarization. When the incoming signal has traveled through the ionosphere (sky wave) the polarization will be random and time-varying due to Faraday rotation effects in the ionosphere. When the incoming signal is due to ground wave propagation, the polarization will be close to vertical.

Similarly, applying the above-mentioned assumption 1, the incident electrical field at the wind farm can be written

$$\mathbf{E}_w(t,\mathbf{r}) = \Re\left\{E_i(t+\tau_d)\mathbf{p}_i e^{j(\omega t - k\mathbf{e}_i\cdot\mathbf{r})}\right\} \tag{3.2}$$

where the only difference is the time difference $\tau_d = d\cos(\phi)/c$. Here, d is the distance between wind farm and receiver site, c is the speed of light, and the angle ϕ is given by $\cos\phi = \mathbf{e}_i \cdot \mathbf{e}_s$, where $\mathbf{e}_s$ is a unit vector pointing in the direction from the wind farm to the receiver site.

The total electrical field incident at the receiver site will be the sum of the incident signal $\mathbf{E}_i(t,\mathbf{r})$ given by (3.1) and the scattered signal $\mathbf{E}_s(t,\mathbf{r})$ from the wind farm:

$$\begin{aligned}\mathbf{E}(t,\mathbf{r}) &= \mathbf{E}_i(t,\mathbf{r}) + \mathbf{E}_s(t,\mathbf{r}) \\ &= \Re\left\{E_i(t)\mathbf{p}_i e^{j(\omega t - k\mathbf{e}_i\cdot\mathbf{r})} + K_s E_i(t-\tau_s)\mathbf{p}_s e^{j(\omega t - k\mathbf{e}_s\cdot\mathbf{r}+\theta_s)}\right\}\end{aligned} \tag{3.3}$$

where K_s is a factor smaller than one, accounting for the signal loss related to scattering as well as to propagation from the wind farm to the receiver site. The phase difference θ_s is due to the different propagation path lengths as well as phase shifts related to the scattering process.

Since the mandate of the work does not include assessing the performance of particular direction finding algorithms, the output from the study should be the parameters describing the relationship between the direct and scattered signal at the receiver site:

- The direction of incidence $\mathbf{e}_i$ and polarization $\mathbf{p}_i$, as well as ω and $E_i(t)$, are parameters describing the incident signal from remote site. For the present discussion these are unknown input parameters.
- The polarization $\mathbf{p}_s$ of the scattered signal is likely to be close to vertical (see discussion below).
- The direction of incidence $\mathbf{e}_s$ of the scattered signal is constant and given by the deployment geometry.
- The multipath time difference $\tau_s = d(1-\cos\phi)/c = d(1-\mathbf{e}_i\cdot\mathbf{e}_s)/c$, directly given by geometrical considerations. For a given deployment geometry this depends only on the direction of incidence $\mathbf{e}_i$, and is upper bounded by $\tau_s \leq 2d/c$. At $d = 40$ km this bound is 0,27 ms.

- The amplitude factor K_s is of high importance in this context, and the main topic of the remaining discussion. It is likely to be easiest to interpret if given in dB units.
- The phase difference θ_s is not likely to be of importance unless K_s is close to 1, and is not discussed further here.

3.2 The amplitude factor

The amplitude factor K_s can be broken up in scattering effects and propagation effects by power budget considerations, giving (derivation details are skipped):

$$K_s^2 = \frac{|E_s|^2}{|E_i|^2} = \frac{4\pi}{\lambda^2}\frac{\sigma(\omega, \mathbf{e}_i, \mathbf{e}_s)}{L(\omega, d)} \tag{3.4}$$

where σ [m^2] is the bistatic radar cross section of the wind farm and L [dimension-less] is the basic transmission loss (by definition incorporating the effective area $A_e = \lambda^2/4\pi$ of an isotropic receiver antenna). In dB units, this is equivalent to

$$\begin{aligned} K_s[\text{dB}] = &-158.55\ \text{dBs}^2/\text{m}^2 \\ &+ 20\log_{10}(f)[\text{dBHz}^2] \\ &+ 10\log_{10}(\sigma)[\text{dBm}^2] \\ &- 10\log_{10}(L)[\text{dB}] \end{aligned} \tag{3.5}$$

3.3 Scattering models

In [1] are presented numerical simulations of scattering from wind turbines, using a MoM (method of moments) program called FEKO. Using a simple geometric model of an 80 m high conical wind turbine tower and a 3-blade rotor with 40 m radius, mounted on a perfectly conducting ground, the simulations predict the bistatic radar cross section σ_1 of a single wind turbine to be as follows:

- At 2-3 MHz, outside resonance: $\sigma_1 \approx 20100\text{m}^2 = 43\text{dBm}^2$
- At the resonant frequency, which is 1.9 MHz for the simulated wind turbine: $\sigma_1 \approx 109000\text{m}^2 = 50\text{dBm}^2$
- At 10 MHz: Between 42 and 48 dBm^2, depending on scattering angle

Let us now consider a wind farm containing N wind turbines. If we make the approximation that the amplitude and phase relationship for the scattering effect from all wind turbines are identical for a given geometry, and disregard mutual coupling and multiple reflections between the wind turbines, we find that the total bistatic radar cross section can be written $\sigma_N = |\chi_N|^2\sigma_1$. The bistatic array factor χ_N is given by

$$\chi_N(\text{RX pos}, \text{TX pos}) = \sum_{i=1}^{N} e^{jk(d_{RX,i}+d_{TX,i}-d_0)}\sqrt{\frac{L(\bar{d}_{RX})}{L(d_{RX,i})}}\sqrt{\frac{L(\bar{d}_{TX})}{L(d_{TX,i})}} \tag{3.6}$$

where $d_{RX,i}$ and $d_{TX,i}$ are the distances from the ith wind turbine to the receiver (transmitter), d_0 is an arbitrary phase reference distance, $L(d_{RX,i})$ and $L(d_{TX,i})$ are the transmission losses between receiver (transmitter) and the ith wind turbine, and $L(\bar{d}_{RX})$ and $L(\bar{d}_{TX})$ are the transmission losses between receiver (transmitter) and a reference point within the wind farm (e.g., its centroid). If the method used in conjunction with Eqns. (3.4)-(3.5), $L(\bar{d}_{RX})$ should be the transmission loss used in the power budget calculation.

Higher-order effects like e.g. multiple scattering or mutual coupling between wind turbines are not included in this analysis. Hence, the predicted fluctuations can not expected to be exact, but the predicted *scale* of the fluctuations should still be close to reality.

If we wish to invoke assumptions 1 and 3 from Sec. 3.1, we set $d_{TX} - d_0 \approx \mathbf{e}_i \cdot (\mathbf{r} - \mathbf{r}_0)$ (where $\mathbf{r}_0$ is an arbitrary reference point) and $L(\bar{d}_{TX})/L(d_{TX,i}) \approx 1$, to obtain

$$\chi_N(\text{RX pos}, \mathbf{e}_i) \approx \sum_{i=1}^{N} e^{jk(d_{RX,i} + \mathbf{e}_i \cdot \mathbf{r} - d_0)} \sqrt{\frac{L(\bar{d}_{RX})}{L(d_{RX,i})}} \tag{3.7}$$

3.4 Propagation models

3.4.1 Free space propagation

In the case of free space propagation with no obstacles within the first Fresnel zone of the straight line between transmitter and receiver, the only "loss" is due to the spherical spreading of the energy, and the basic transmission loss is given by

$$L(\omega, d) = \left(\frac{4\pi d}{\lambda}\right)^2 \tag{3.8}$$

where d is distance.

3.4.2 Ground wave propagation

Since the Earth's surface will generally be within the first Fresnel zone of the direct path at frequencies in the HF range, the free space propagation model is not valid. The propagation effect along the surface in this case is called "ground wave", and is a combination of free space propagation above ground and Sommerfeld-Norton surface-bound wave [6, 7]. The ground wave path loss depends on the conductivity and permittivity of the ground, and curves are given in Rec. ITU-R P.368-7 [5] for some ground types (sea water, wet ground, dry ground, very dry ground, ...). The program GRWAVE, downloadable free of charge from ITU-R, can be used to compute the ground wave path loss for any combination of conductivity and permittivity.

The ground wave path loss curves generally exhibit a region close to the transmitter following the free space formula (20 dB/decade), an intermediate region where the path loss increases by approximately 40 dB/decade, and a cutoff distance above which the path loss increases very rapidly. For the case of sea water, the path loss is within 3 dB of the free space formula for

frequencies up to 10 MHz at distances up to 40 km. For the case of very dry ground, the path loss is 10 dB higher than free space at 2 MHz at 1 km distance (the difference increases with increasing frequency and with increasing distance).

As a rule of thumb, ground wave is applicable at ranges up to about 50 km over land and 500 km over sea, the exact range being dependent on frequency, transmitter and receiver equipment, and ground properties.

The polarization $\mathbf{p}$ associated with ground wave propagation is close to vertical when propagating over sea, and sligtly skewed (also having a horizontal component in the direction of propagation) when propagating over land where losses are higher.

One problem with applying the GRWAVE method is the selection of proper ground parameters, which depend on the amount of water in the ground.

In the case of ground parameters varying along the propagation path (e.g., crossing a fiord), first order approximations are to apply average representative parameters for the path or local parameters at receiver or transmitter site, while more exact performance can be achieved by applying a method called “Millington’s method”, as an extension to GRWAVE (see e.g. Annex 2 of [5]). FFI has a Matlab implementation of Millington’s method [4].

In the case of distinct topographic features between transmitter and receiver, like a big mountain or deep valley, the GRWAVE result will be inaccurate. The exact prediction of path loss under such circumstances is not a mature field [4], but in general a mountain will increase the path loss while a valley will lead to lower path loss (closer to free space).

Under no circumstances will the path loss of ground wave propagation be smaller than that of free space propagation. Hence, the free space path loss given by (3.8) can be taken as the lower limit for L. This limit is close to the actual path loss if propagation is over sea or across a deep valley, but far from reality in other cases.

3.4.3 Sky wave propagation

At distances above approximately 50 km over ground or 500 km over sea, the dominant propagation mechanism in the HF frequency range is refraction from the ionosphere, called sky wave propagation. The refractive layers are in the range 100-300 km above ground. At distances above approximately 4000 km, the only propagation mechanism supported is multihop sky wave propagation (including ground reflections) due to geometric considerations.

The path loss associated with sky wave propagation depends on frequency, and the state of the ionosphere, which is a complex system varying with time of day, time of year, and solar and geomagnetic activity. Predicting the path loss of sky wave propagation is not deemed necessary for the present work.

The polarization of sky waves is randomized by Faraday rotation effects, due to the presence of the Earth’s magnetic field in the ionosphere [3].

Sky wave is the dominant propagation mechanism for signals from remote transmitter sites, but is likely to be negligible compared to ground wave for propagation from the wind farm to

receiver site in our present discussion, at least for vertically polarized scattering. Short range sky wave propagation is called NVIS (near vertical incidence sky wave), and the associated path loss is lower bounded by inserting $d = 200$ km (the minimum distance to the ionosphere and back) into the free space equation (3.8). Additional to this comes refraction and absorption losses in the ionosphere (comparison with the sky wave prediction program ICEPAC indicates that these additional terms sum up to between 15 and 30 dB). For horizontally polarized scattering one should estimate the NVIS loss as well as the ground wave loss in order to identify the dominant propagation mechanism. For NVIS scattering, the incoming direction $\mathbf{e}_s$ of the scattered signal at the receiver site will have a vertical component which is stronger than the horizontal component in the direction from the wind farm.

3.5 Application to scenarios

The discussion above is general. When evaluating specific scenarios, values of σ and L should be estimated and used in equation (3.5).

4 MEASUREMENT CAMPAIGN AT SMØLA

A measurement campaign was performed at the island of Smøla, June 6-8 2006, in order to obtain real-world experience with HF scattering effects from wind turbines. The largest wind farm on land in Europe is located at Smøla (information from 2005).

The planning period for the measurement campaign extended over only a few weeks, and the team had no prior experience in measuring HF scattering from wind turbines. One can therefore in hindsight obviously spot things that should have been done differently. Nevertheless, an interesting data set was collected, to be described in detail below.

The objective of the measurement campaign was to identify scattering effects from the wind farm believed to be strongly sensitive to geometry (due to constructive/destructive interference patterns caused by the large number of reflectors), or time-varying effects due to scattering and/or shadowing being modulated by the blade rotation of the wind turbines.

The general concept of the measurement campaign is as follows: A transmitting HF radio is mounted on a boat, traversing different trajectories to obtain different transmitter-receiver geometries relative to the wind farm. At the receiver site, an interferometer consisting of two spatially separated vertical antennas is used as a simple direction finding station. As the transmitter moves, any angle- (or time-) dependent scattering from the wind farm should be evident as fluctuations in the phase difference between the two receiver antennas.

4.1 The wind farm at Smøla

The wind farm at Smøla is operated by Statkraft AS. It contains 68 wind turbines, each with a total height of 110 m (70 m tower + 40 meter blade radius). The park is located in the Northwestern part of Smøla covering an area of approximately 4 x 4 km. The location of each wind turbine is shown in the map in Fig. 4.1.

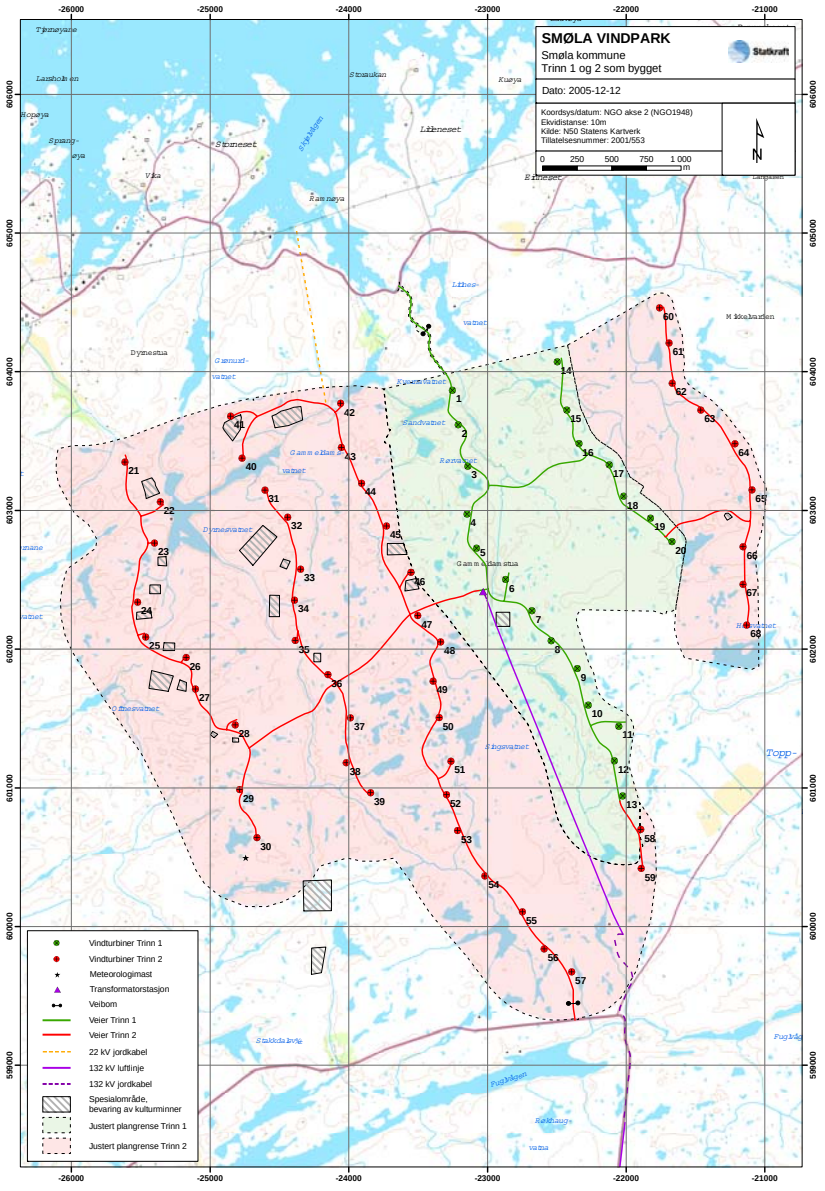

Figure 4.1 Wind turbine locations at Smøla. Map provided by Statkraft AS.

Day	Time	Rotation rate
Tuesday June 6	15-19	11 RPM
Wednesday June 7	12-15	17 and 16.6 RPM
	15-16	11 RPM
	16-17	17 and 16.6 RPM
Thursday June 8	8-16	11 RPM

Table 4.1 Shaft rotation rates of wind farm during campaign.

The wind farm has two different gears of operation, where the shaft rotation rate is 11 or 17 RPM (revolutions per minute) for mills 1-20 and 11 or 16.6 RPM for mills 21-68, according to Statkraft. The rotation rates are synchronized to the 50 Hz line frequency, but the different wind turbines do not rotate in phase. Each wind turbine has three blades, such that 11 RPM corresponds to a blade frequency of 0.55 Hz, 16.6 RPM corresponds to 0.83 Hz and 17 RPM corresponds to 0.85 Hz.

The rotation rates during the campaign were as shown in Table 4.1, according to Statkraft. Fig. 4.2 shows how the rotation rate of one wind turbine varied when switching between high and low gear on June 7th, where we observe that the rotation rate is changing gradually and not abrupt.

4.2 Transmitter equipment

The transmitter was a Yaesu FT-840 amateur radio station with temperature controlled crystal oscillator (TCXO) TCXO-4 installed. The transmitter antenna was a 5 m long vertical antenna VB-500 from DXSR Antennas. This antenna is equipped with a broadband impedance transformer at the feed point, and can operate as transmit antenna in the range 3.5-30 MHz without an antenna tuner (SWR$< 1.8:1$ relative to 50 ohms) and 1.8-52 MHz with an antenna tuner. The antenna gain as function of frequency is shown in Fig. 4.3. The antenna efficiency is reduced below 3 MHz, but the signal was still clearly audible on the receiver for all geometries throughout the campaign. An automatic antenna tuner of type LDG Z-100 was used as matching between the transmitter and the antenna.

The antenna was mounted on a rib (rigid inflatable boat), with the radio, antenna tuner, and laptop computer for GPS logging placed in an aluminum container on board. The boat was capable of running at 21.6 m/s (40 knots), but was operating at speeds in the range 5-15 m/s throughout the campaign. Fig. 4.4 shows the transmitter boat in operation. On the first day of the campaign the antenna broke after about two hours due to mechanical stress. The next morning it was refitted with parts from the receiver antennas, and fastened with guys (as seen in the picture) to decrease the mechanical load on the antenna.

During each run, an unmodulated carrier wave was transmitted continuously at a single operating frequency. The transmit power was 10 W on Tuesday June 6th and 50 W during the remainder of the campaign. The position of the boat during the campaign was logged by GPS.

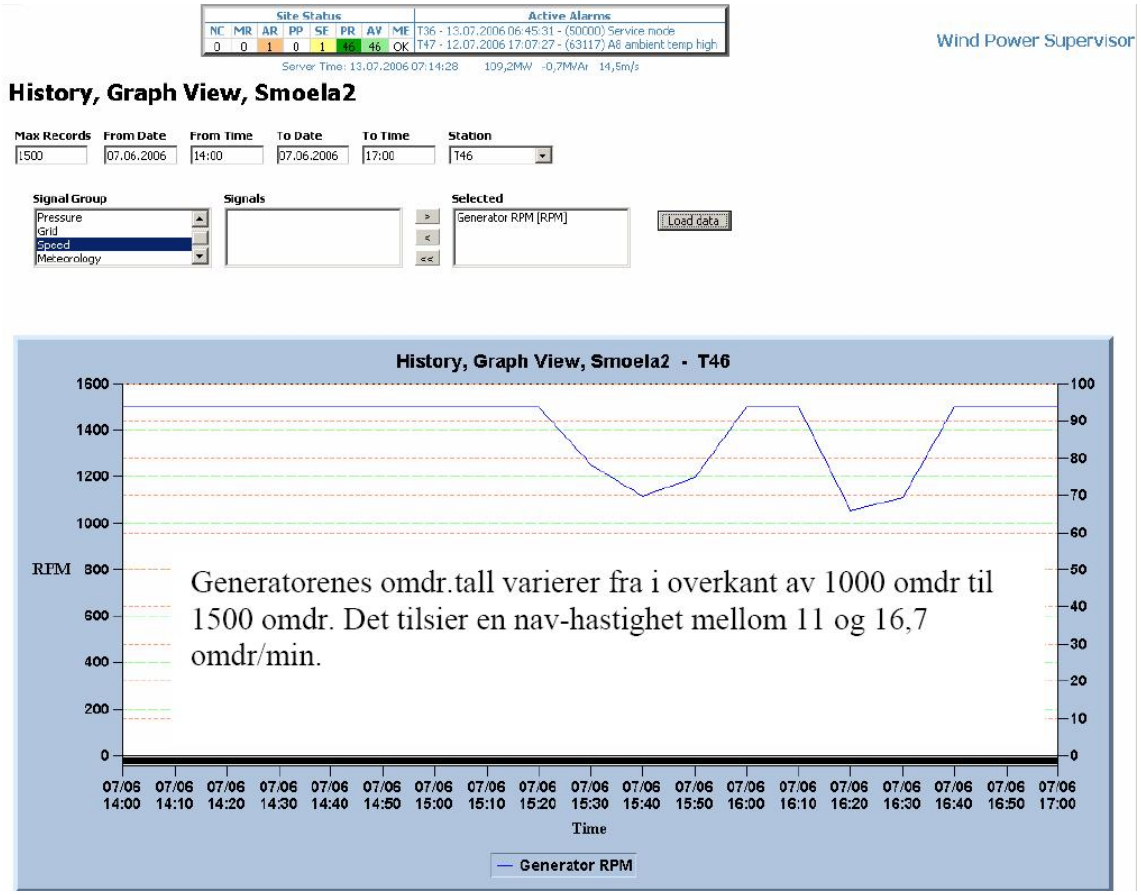

Figure 4.2 Shaft rotation rate of one wind turbine on June 7th. Figure provided by Statkraft AS. 1000 RPM generator speed corresponds to 11 RPM shaft rotation rate, and 1500 RPM to 16.7 RPM.

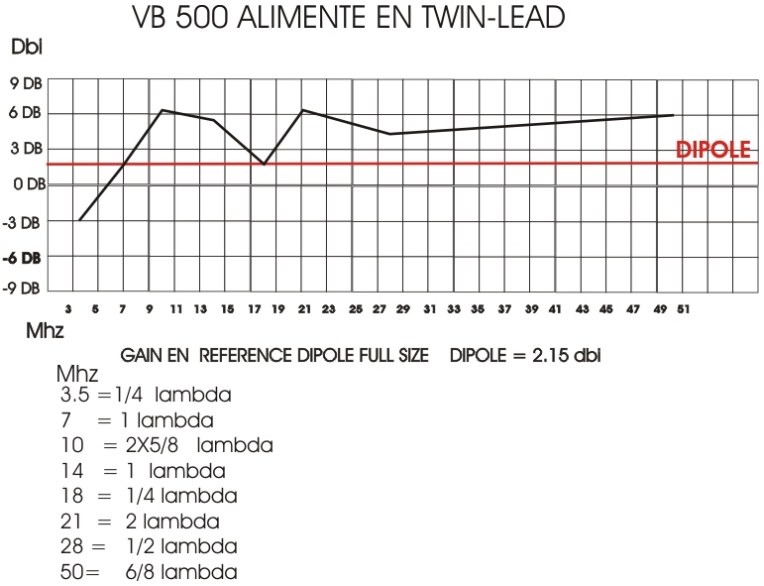

Figure 4.3 Antenna gain of VB-500 antenna, from http://www.dxsr-antennas.com.

Figure 4.4 Transmitter boat in operation.

4.3 Receiver equipment and instrumentation

The receiver station measured the phase difference between two vertical antennas with a horizontal separation of 100 m. This was accomplished using two phase-synchronized Yaesu FT-840 amateur radio stations with 500 Hz CW filters installed. The phase synchronization was achieved by using the same TCXO-4 as reference oscillator for both radios (the TCXO was installed in one radio and the oscillator signal passed to the other radio through a cable). With both radios tuned to the same receiver frequency, this caused the phase locked loops (PLLs) of the two radios to be phase-synchronized to within an arbitrary offset in phase difference.

Figs. 4.5-4.6 show the measurement setup. The audio signals (demodulated side tones) output from both radios were connected to an HP3575A gain/phase meter measuring the phase difference between the two sinusoids. The measured phase difference can be monitored on a digital display, and is also output as an analog voltage proportional to the phase difference.

Data acquisition was performed using a National Instruments DAQPad-6015, connected to a laptop computer via USB interface. Three single-ended (ground-referenced) analog input channels of the DAQPad were used, one connected to the analog output of the gain/phase meter and the other two connected to the AGC (automatic gain control) voltage of each radio.

The original plan for data acquisition failed due to software problems, and an improvised solution was implemented using a Labview program originally designed for another purpose. The DAQPad was configured to sample at a nominal rate of 2000 samples/second with 16 bits/sample, and the Labview program filtered the data with a 4th order lowpass Butterworth filter with cutoff frequency at 2 Hz, before saving to disk as 32-bit floating point numbers at a nominal rate of 10 samples/second. Unfortunately, the clock synchronization input of the

Figure 4.5 Receiver measurement equipment, mounted in the back of a Volkswagen Transporter and powered by a Honda generator.

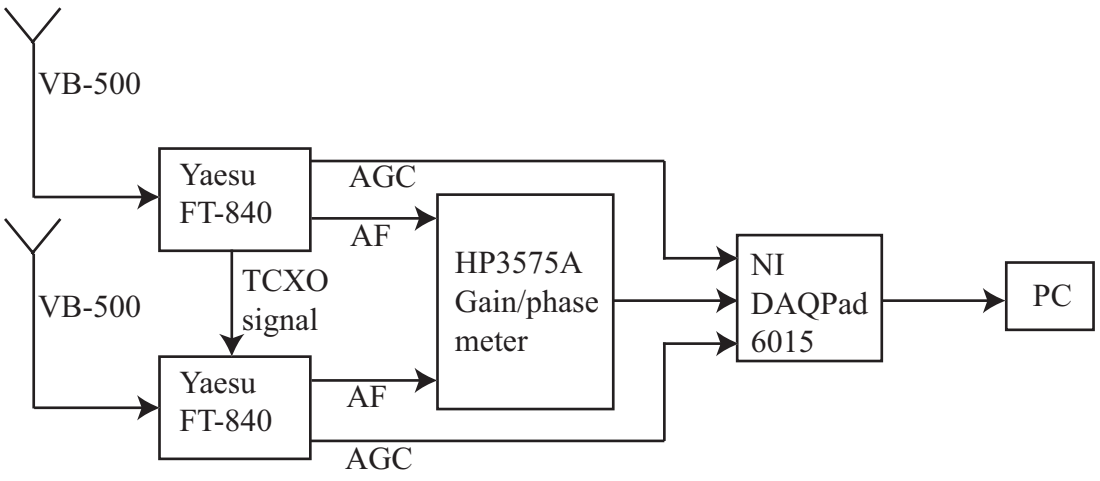

Figure 4.6 Receiver measurement setup.

DAQPad was not used, and post-processing reveals that the nominal sampling rate was quite inaccurate (see Sec. 4.6).

During two of the runs the improvised data acquisition solution was not operational (see Table 4.2), and logging was done manually by writing down the phase difference from the meter display every 10 seconds.

The logged AGC voltages turned out to be very informative, as there were sheep fences present in the area which emitted broadband noise bursts about once a second, causing slight fluctuations in the measured phase difference. The noise bursts from sheep fences are clearly indicated in the AGC voltage.

Laboratory measurements at a frequency of 2.692 MHz prior to the campaign show that the AGC voltage of the radios is constant at 9 mV for input levels lower than -110 dBm, and increase at a rate of 27 mV/dB up to -80 dBm before flattening out again, as shown in Fig. 4.7. These measurements also reveal that the measured phase difference varies with $\pm 3\,^\circ$ as function of received signal level.

Further laboratory measurements were made after the campaign, but are not presented here as they do not counter the general conclusion that the phase difference measurement setup is stable, and does not vary by more than a few degrees as function of signal level (as long as the signal is strong enough to be demodulated, above about –130 dBm). This was also confirmed for the case were the signal level to one radio was kept constant while varying the received signal level at the other radio.

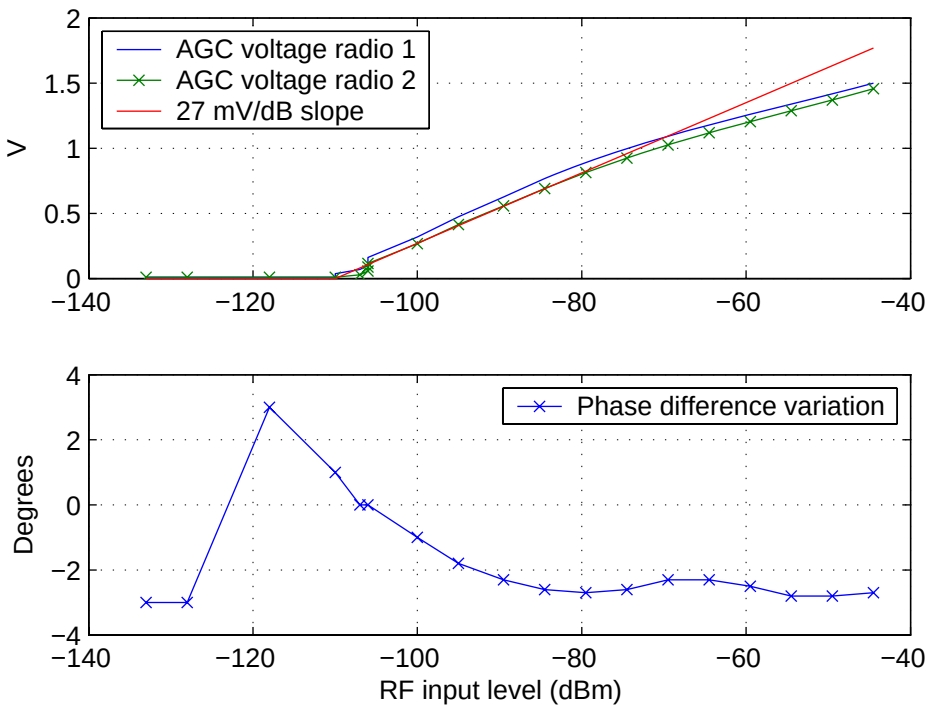

Figure 4.7 *Laboratory measurements of phase-synchronized Yaesu-840 receivers at 2.692 MHz, showing AGC voltages and phase difference variation as function of input level.*

Measurement data from the campaign indicate that the drift with time in the measured phase difference is on the order of 0.14 degrees/minute (see Sec. 4.10).

The two receiver antennas were of the same type as the transmitter antenna, VB-500. After the transmit antenna broke the first evening and was refitted with parts from the receiver antennas, the receiver antenna lengths were approximately 2.5 m and 3.75 m, respectively (each antenna consisted of 4 parts, and 3 parts of the transmitter antenna were lost into sea).

The antenna positions are shown in Fig. 4.8. The first day the antennas were mounted at the pre-planned site, but for various reasons (e.g., a power line crossing right over the interferometer) the receiver site was moved further East for the remainder of the campaign. On Tuesday the antenna separation was 95.2 m $\pm\, 0.2$ m and the broadside direction was $-60° \pm 5°$ relative to North. The remaining days the antenna separation was 100.0 m $\pm\, 0.2$ m and the broadside direction was $-29.3° \pm 0.2°$ relative to North.

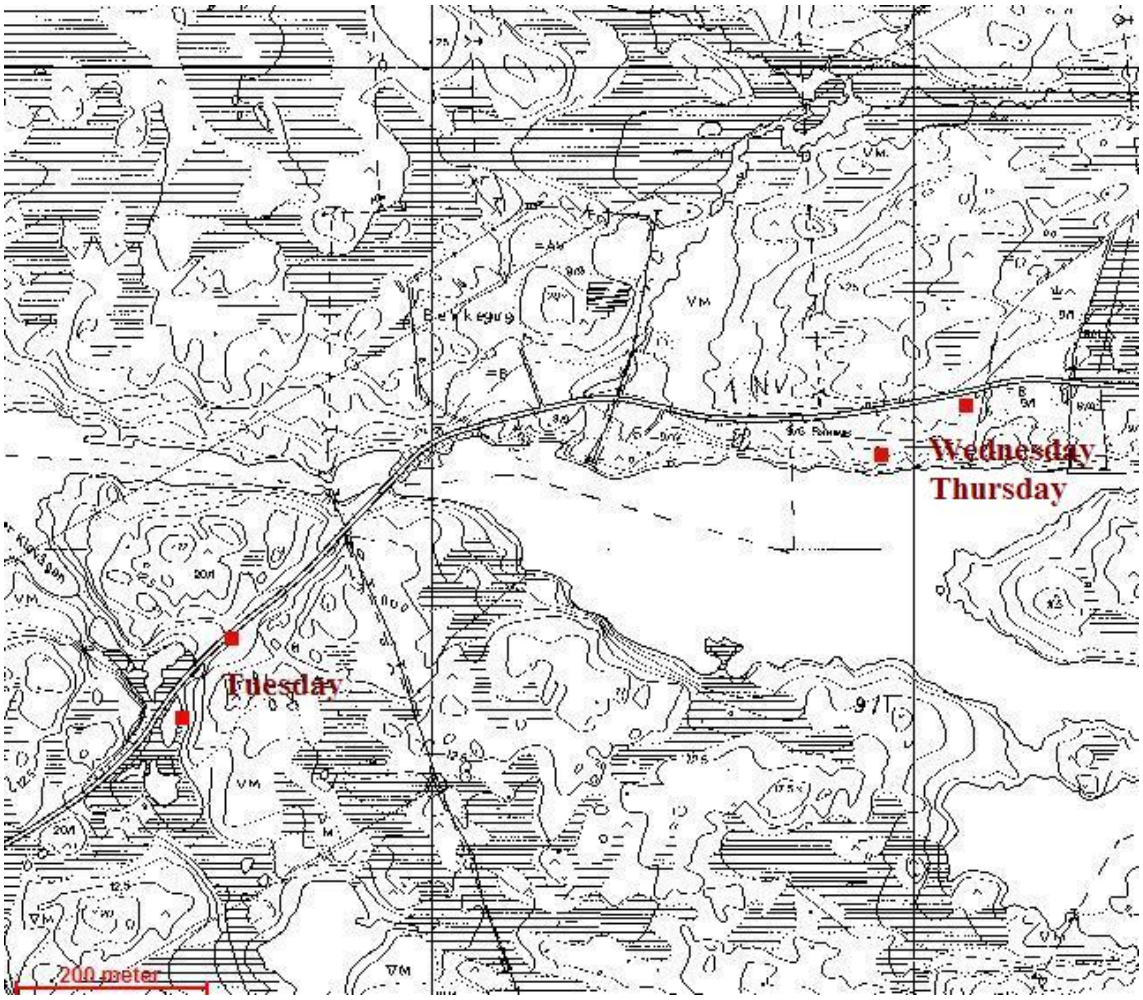

Figure 4.8 Map showing receiver antenna positions on Tuesday June 6th (left) and Wednesday-Thursday June 7th-8th (right). The area is a few km East of Straumen in the Southeastern part of Smøla.

4.4 Campaign overview

The locations traversed by the transmitter boat throughout the campaign are shown in Fig. 4.9. A number of way points S0-S20 were defined to ease communication. The home quay of the boat was at position S0.

An overview of the operations during the campaign is shown in Table 4.2. A total of nine operating frequencies were assigned (five in the range 2-3 MHZ, two around 10 MHz, and two around 30 MHz), but only three of the frequencies were used when the boat was in motion. In run 9, there were performed measurements at all nine frequencies with the transmitter stationary at quay at S0.

Figure 4.9 Map showing the locations of the transmitter boat throughout the campaign. S0-S20 are way points which were used for operational reference.

During run 2 the transmitter went silent in the periods 1443-1453 and 1503-1508 due to a loose connector. Automatic data acquisition was operational during all runs except 1 and 4.

The operations at 2.212 and 9.991 MHz are also plotted directly in the map in Figs. 4.32-4.33 in Sec. 4.15.

There are mountains of up to about 400 m height at the other side of the fiords East and South of Smøla. Some km further South (outside the map in Fig. 4.9) are mountains of about 900 m height. Some of these mountains may have caused natural scattering effects in the experiment.

Day	Run #	Local time	MHz	Logging	Transmitter movement
Jun 6	1	1741-1933	2.212	Manual	S0-S7 in open waters
Wed	2	1410-1601	2.212	DAQPad	S0-S8 in open waters
Jun 7	3	1602-1649	2.833	DAQPad	S8-S0 close to shore
	4	0829-0918	2.833	Manual	S0-S17 in open waters
	5	1020-1120	2.212	DAQPad	Close to shore inside S16-S19, stopping to fill gas
Thu	6	1121-1151	9.991	DAQPad	Close to shore inside S19-S0
Jun 8	7	1242 -1324	2.212	DAQPad	Close to shore inside S0-S9
	8	1329-1405	9.991	DAQPad	Close to shore inside S9-S0
	9	1405-1505	Various	DAQPad	At quay, S0, transmitting 5 minutes each freq

Table 4.2 Overview of measurement campaign at Smøla. Positions refer to the way points in Fig. 4.9.

4.5 Computing distances and angles

The receiver position, and the log of transmitter positions, were recorded as GPS coordinates in the WGS84 datum, with 5 m uncertainty. The wind turbine positions were given in UTM32 coordinates, which we converted to the WGS84 datum. To compute distance and bearing (angle of arrival) between points we used a very accurate iterative algorithm by Vincenty [9] based on the WGS84 reference ellipsoid (a simple flat Earth approximation could not be used, as it turned out to have an inaccuracy of up to 300 m over the operating area).

4.6 Receiver time synchronization

As described in Sec. 4.3, the data acquisition hardware was not provided with proper clock synchronization, such that there is no guarantee that the nominal sampling rate of 10 Hz in the saved files is correct.

To synchronize the measurements to the transmitter GPS data, we investigated events during the campaign when the boat did maneuvers (changing direction, starting, or stopping). At such events, the change in gradient in measured phase difference should appear at the time instant when the maneuver took place.

It was found that assuming the sampling rate of the measurement data files to be 10.627 Hz throughout the campaign led to good agreement between phase difference measurements and GPS log for all such events. A subjective judgment of the different events suggests a residual uncertainty in the timing of about 10 s.

4.7 Interferometer calibration

It is easy to show that when an electromagnetic plane wave is incident at a two-antenna interferometer from a horizontal direction, the phase difference (in radians) should be

$$\phi = kd \sin \alpha \tag{4.1}$$

where $k = 2\pi/\lambda$ is the wave number, d is the antenna separation, and α is the angle of arrival relative to broadside. Note that the slope $d\phi/d\alpha$ varies between $\pm kd$ in the broadside directions and 0 in the endfire directions.

The receiver equipment measured the phase difference between the two antennas, with an unknown offset which was relatively constant as long as the receiver frequency was not changed. From the GPS log we obtain the incidence angle α as the boat moves, and we can compare the actual measured phase difference with the theoretical phase difference predicted by (4.1), disregarding the unknown offset and investigating the slope only.

All measurements at 9.991 MHz show good agreement between the measured and theoretical phase difference slope. But at 2.212 MHz and 2.833 MHz it turns out that the slope is completely wrong. To make the measurements reasonable, we need to calibrate the interferometer by replacing k in (4.1) by an effective wave number $k_{eff} = k/\eta$. The calibration factor η, for the receiver site used on June 7-8, is estimated to be (based on a combination of least squares fits and subjective judgment):

- $\eta \approx 0.59$ at 2.212 MHz, when transmitter is North or South of Smøla (between S0 and S8 and between S15 and S16-17, behind Edøya).
- $\eta \approx 0.98$ at 2.212 MHz, when transmitter is East of Smøla (between S16-17 and and S19, close to shore).
- $\eta \approx 0.775$ at 2.833 MHz, when transmitter is North of Smøla (between S0 and S8).
- $\eta \approx 0.9$ at 2.833 MHz, when transmitter is East of Smøla (between S0 and S17).
- $\eta = 1$ at 9.991 MHz regardless of transmitter position; interferometer is operating according to theory without calibration.

Note that we always observe $k_{eff} > k$, corresponding to a decrease in wavelength compared to the nominal value of c/f.

On Tuesday June 6, at another receiver site farther from shore (see Fig. 4.8), $\eta = 1$ gives good agreement between theory and measurements at 2.212 MHz, hence there is no need to calibrate the interferometer at that site.

Several hypotheses have been evaluated to explain the apparent change in wave number in the frequency range 2-3 MHz:

- **Influence from wind farm:** We find no way to explain the error in interferometer phase slope by scattering from the wind farm. Conclusion: **Not probable.**

- **Sky wave propagation:** If propagation happened to be via sky wave rather than ground wave, the signal would arrive from a high elevation angle that would change the apparent horizontal wave number. However, path loss predictions for the actual geometries indicate that the ground wave signal should be at least 25 dB stronger than the sky wave signal. Also, an elevation angle different from zero would cause the apparent horizontal wave length to increase rather than decrease. Conclusion: **Not possible.**

- **Decreased propagation velocity:** One could argue that the propagation speed of ground waves would be lower than the speed of sound c in free space, since part of the energy is absorbed into the ground and the propagation velocity in the ground is lower than in free space (by a factor $\sqrt{\epsilon}$). However, a literature search does not reveal a single reference supporting this, and the original derivations of ground wave propagation (e.g., [7]) do not include any terms that would significantly increase the wave number. Also, the fact that the interferometer did not require calibration at the site farther from shore counters this hypothesis. Conclusion: **Not probable.**

- **Reflection from ground-sea boundary:** The interferometer antennas were located close to a strait of sea water, approximately 20 m and 65 m from shore. The conductivity contrast between ground and sea water is approximately three decades, and also the permittivity is different. This discontinuity in ground impedance will cause the propagating ground wave to be reflected at the boundary. According to [10], severe phase variations can be expected at distances close to shore (relative to the wavelength), and these phase variations will be a function of the angle of incidence on the boundary. This fits our observations, for the following reasons: (a) η is close to 1 at 10 MHz, where the distance to shore measured in wavelengths is longer. (b) η is farther from 1 at 2.212 MHz than at 2.833 MHz, and also depends on the angle of incidence. (c) η is 1 at 2.212 MHz when the interferometer is located farther from shore (Tuesday, see Fig. 4.8). Conclusion: **Likely cause.**

It is not clear whether the reflections from the ground-sea boundary would cause small-scale fluctuations in η as function of angle of incidence, which (if present) might be mistaken as phase difference fluctuations caused by the wind farm. By geometrical considerations, small-scale fluctuations in η are more likely when the signal arrives along the shore (near the the array endfire direction) than across the shore (near the array broadside direction). For this reason, the interferometer calibration is better (i.e., k_{eff} appears to be constant) for signals arriving from the North/South than from the East/West.

One should also be aware of the theoretical possibility that the calibration procedure may have removed some effects which in reality are due to the wind farm.

At 9.991 MHz the ground-sea boundary does not seem to influence the measurements, and is hence unlikely to be a source of error in the interferometer measurements.

4.8 Fingerprint prediction

When phase fluctuations are observed in the measurements, an obvious question is whether these are caused by scattering from the wind farm, or by other natural effects. One indicator is

to compare it with a predicted “fingerprint” of the wind farm, given by evaluating the amplitude and phase of the array factor in Eq. (3.6) for all positions in the transmitter GPS log. Note that assumptions 1 and 3 from Sec. 3.1 do not hold for the campaign geometries, such that the simplified Eq. (3.7) should not be used for this purpose.

For all runs, the array gain and phase were computed as function of time. For this purpose, the transmission loss used in Eq. (3.6) was assumed to be proportional to $d^{4.1}$ (41 dB/decade), which from the GRWAVE program is found to be a typical value for ground wave propagation over land (this will be slightly inaccurate for the transmitter-wind turbine path, which propagates partly over sea before entering land).

One should keep in mind that due to the number of idealizations in the model, the predicted array factor can not be expected to be an exact estimate of the fingerprint of the wind farm. Nevertheless, it should give a good indication on the periodicity that can be expected in phase difference fluctuations.

An approximate value of the “array gain” caused by the wind farm geometry (the equivalent number of wind turbines of which the scattering effects are added in phase) can be estimated by ignoring all loss terms in Eq. (3.6). Between 2 and 3 MHz, this approximated value of $|\chi_N|$ varies between 30 (30 dB) and 10 (20 dB) when the wind farm is between the transmitter and receiver, and between 20 (26 dB) and 0 otherwise. At 10 MHz, it varies between 20 (26 dB) and 0.

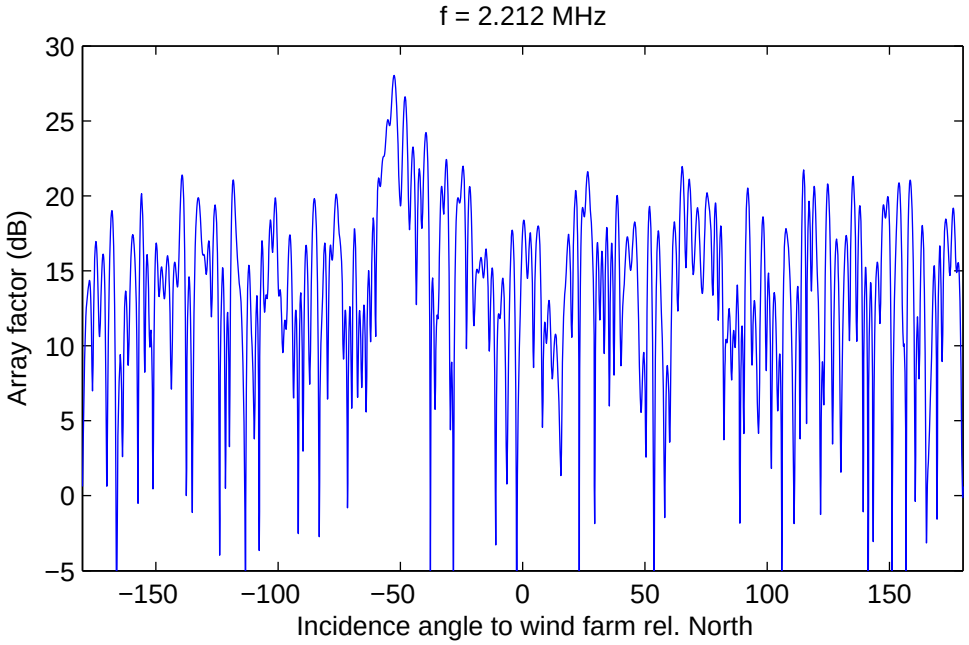

Figure 4.10 Amplitude variations of predicted fingerprint at 2.212 MHz.

The predicted wind farm fingerprints for the receiver position used in the campaign are shown in Figs. 4.10-4.11, at the frequencies 2.212 and 9.991 MHz, respectively. These figures are for the case where the transmitter is so far away from the wind farm that the incoming signal can be modeled as a plane wave, such that Eq. (3.7) can be applied, and are shown as function of angle of incidence *referred to the wind farm* (as opposed to figures later in the report which are

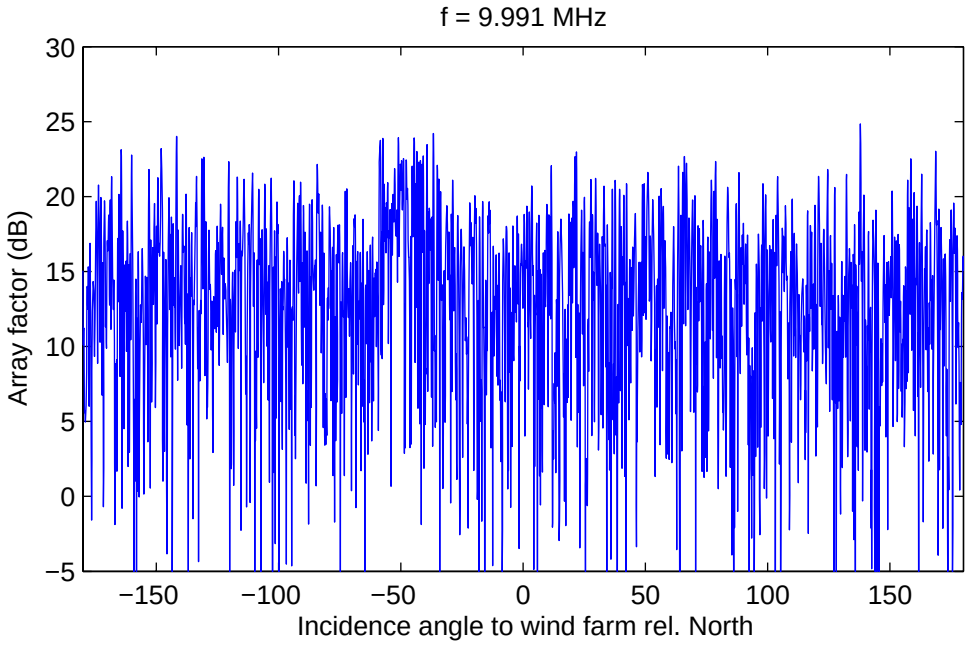

Figure 4.11 Amplitude variations of predicted fingerprint at 9.991 MHz.

referred to the receiver position). We note that, in particular at the lower frequency, a focusing effect is predicted when wind farm is between transmitter and receiver (note that the model does not take possible shadowing effects into account). Also, the model predicts fluctuations as function of angle, which are faster at the higher frequency. At 2.212 MHz, the predicted focusing effect is about 10 dB higher than the fluctuations at other angles, and exhibits an abrupt transition to the West and a soft transition to the East.

The modelling presented above is for an elevation angle of zero, e.g. groundwave propagation. Repeating the modelling for higher elevation angles, it is seen that the predicted focusing effect behind the wind farm may be present for elevation angles up to about 10 degrees. This is of relevance when considering sky wave propagation from far away, which has *not* been covered by the present measurement campaign.

4.9 Expected signature from terrain

In the HF frequency band reflections from the terrain are dominated by large scale variations in surface slope and conductivity profiles. These scales will be present ranging from those given by the local wave number (e.g. 100 m wave length in the lower HF band) to those given by the largest scale variations, such as the distance between dominant terrain features (e.g. 50 km in a given scenario). The relative contribution of these scattering scales can be best be assessed using the k^{-n} law which has been found to represent a large number of natural geophysical features ranging from oceanographic turbulence patterns to topographic surface variations and ionospheric variations [2]. For two-dimensional surface variations $n = 7/3$ has been found to be the most commonly encountered parameter. An example spatial wave number distribution of this form is shown in Fig. 4.12.

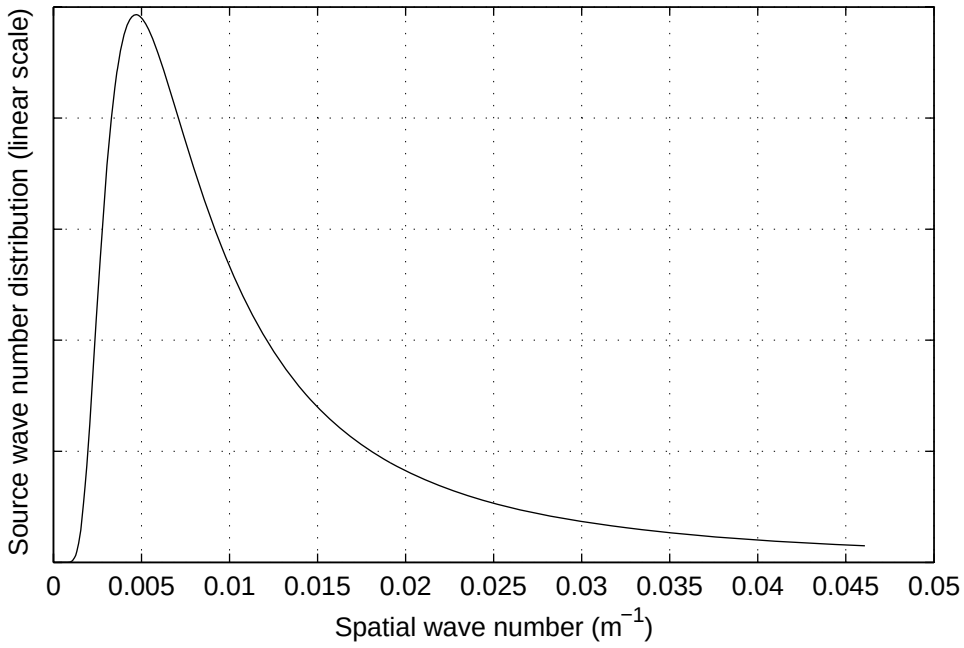

Figure 4.12 A typical assessment of terrain scattering (source) spatial wave number distribution ($n = 7/3$), 1300 m maximum cutoff scale.

Although this distribution only represents average and simplistic cases, the typical angular responses may be calculated to indicate the type of responses expected for given terrain formations and ranges of terrain to transmitting and receiving sites. This will give indication as to the expected type and magnitude of variations, and will assist in the manual interpretation of data. Examples are shown in Fig. 4.13.

4.10 Measurements with stationary transmitter

During parts of the campaign the boat was in a stationary position with the transmitter operational. These measurements can be used to estimate instrumentation noise and natural noise in the measured phase difference.

While the boat was filling gas at Vikan during run 5, the received signal level was strong due to the short distance, and there was little noise (about 0.1 degrees RMS). In this time interval, we observed a drift in the measured phase difference of 0.14 degrees/minute. This can be used as an estimate of the stability of the phase difference between the two synchronized receivers.

A number of measurements were performed with the transmitter stationary at quay in position S0. These are summarized in Table 4.3. We note that the noise from sheep fences gives rise to phase difference fluctuations of 1.5 degrees RMS or lower, at a frequency of 0.92 Hz.

On June 8, fluctuations with 3 seconds period and up to 2.3 degrees RMS are observed at 2.833 MHz and above, but not at 2.692 MHz and below. These fluctuations were not observed at 2.833 MHz the day before with the transmitter in exactly the same position (the wind was markedly stronger on June 8 than on June 7). Also, the fluctuations come together with an

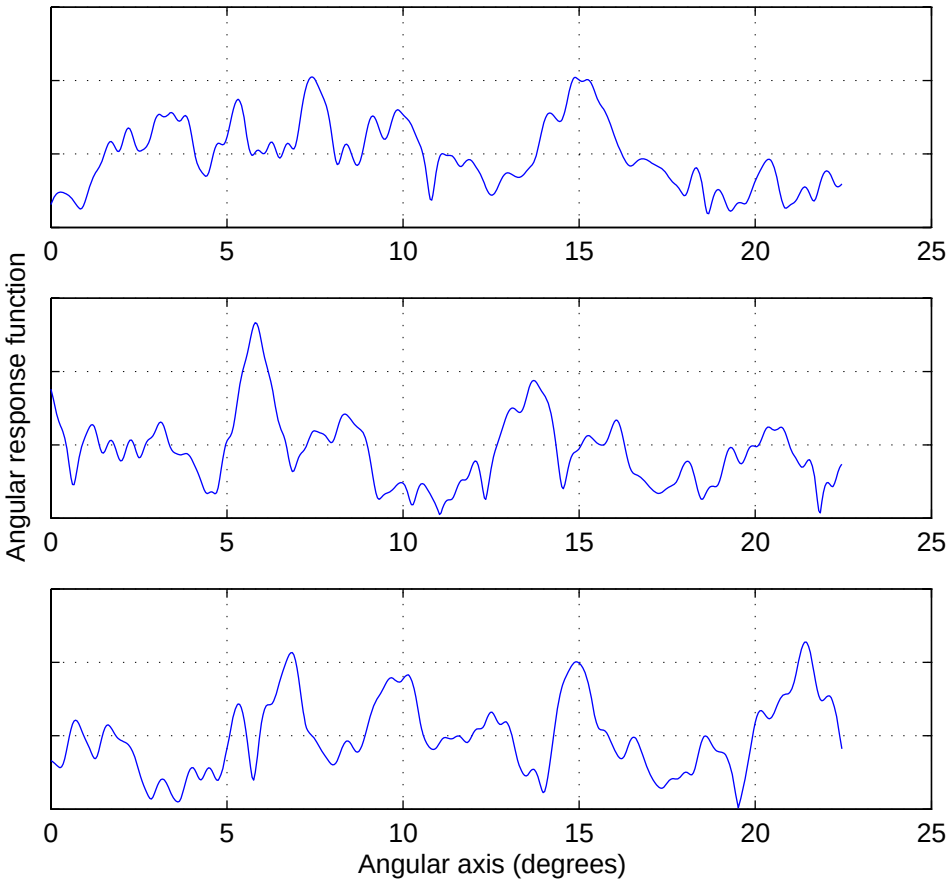

Figure 4.13 Sample simulated realizations of terrain reflections. Scale and typical patterns may be used for pattern recognition, angular response may be extracted from data fitting to measurement data.

increased AGC voltage, fluctuating coherently with the phase difference, at the radio connected to the antenna closest to shore. The reasons for these fluctuations have not been studied in detail, but one reason might be Bragg resonant scattering from waves on the sea surface.

MHz	Time	RMS phase fluctuation	Dominant frequency
2.212	June 8, run 9	1.0 degrees	0.92 Hz, coherent with sheep fences
2.479	June 8, run 9	1.4 degrees	0.92 Hz, coherent with sheep fences
2.692	June 8, run 9	1.5 degrees	0.92 Hz, coherent with sheep fences
2.833	June 7, end of run 3	1.4 degrees	0.92 Hz, coherent with sheep fences
2.833	June 8, run 9	2.3 degrees	0.33 Hz, narrow-banded
9.991	June 8, end of run 6	1.9 degrees	0.33 Hz, narrow-banded
9.991	Jun 8, run 9	2.3 degrees	0.33 Hz, narrow-banded

Table 4.3 Overview of measurements with boat stationary at quay (S0).

From these measurements we can conclude that fluctuations higher than 1.5 degrees RMS are not likely to be due to instrumentation noise or sheep fences, and on June 8, fluctuations higher than 2.3 degrees RMS are not likely to be related to the 0.33 Hz fluctuations of unknown origin. Fluctuations at frequencies different from 0.92 Hz or 0.33 Hz are not likely to be related to any of these noise sources.

4.11 Angular sweeps at 2.212 MHz

In Figs. 4.14-4.17 we present measurements where the transmitter performed angular sweeps with approximately constant TX-RX distance, with transmitter frequency of 2.212 MHz. In each figure, the upper and lower plots have identical time scales even though the upper plot is annotated by angle of arrival (AOA). Each figure spans a time interval where the AOA has been swept close to linearly and the measured phase difference does not wrap between ± 180 degrees. Note that the x-axes (time and angular scales) are different for the different figures.

At 2.212 MHz, with the transmitter South of Smøla (Fig. 4.16), there are phase fluctuations of about 15 degrees with periodicity of about 12.5 seconds (corresponding to 1 degree in AOA). In this geometry, the fluctuations are not likely to be caused by scattering from the wind farm unless it exhibits very strong backscattering, since the 10 km path between the receiver and wind farm, with transmission loss of approximately 80 dB each way, would have to be traversed back and forth. Other possible explanations are natural scattering effects (e.g., mountains), or small-scale angle-dependency of the calibration factor η due to the interferometer being too close to shore (see Sec. 4.7). Theoretical considerations on the scale of the fluctuations do however not support the latter hypothesis.

At 2.212 MHz, with the transmitter passing behind the wind farm close to shore (towards the right in Fig. 4.17), there are phase fluctuations of about 15 degrees with periodicity of 30-100 seconds (corresponding to 1-3.6 degrees in AOA). These fluctuations may be due to the wind turbines, as the periodicity is on the same time scales as in the predicted array factor. The level of the fluctuations is, however, approximately as in Fig. 4.16.

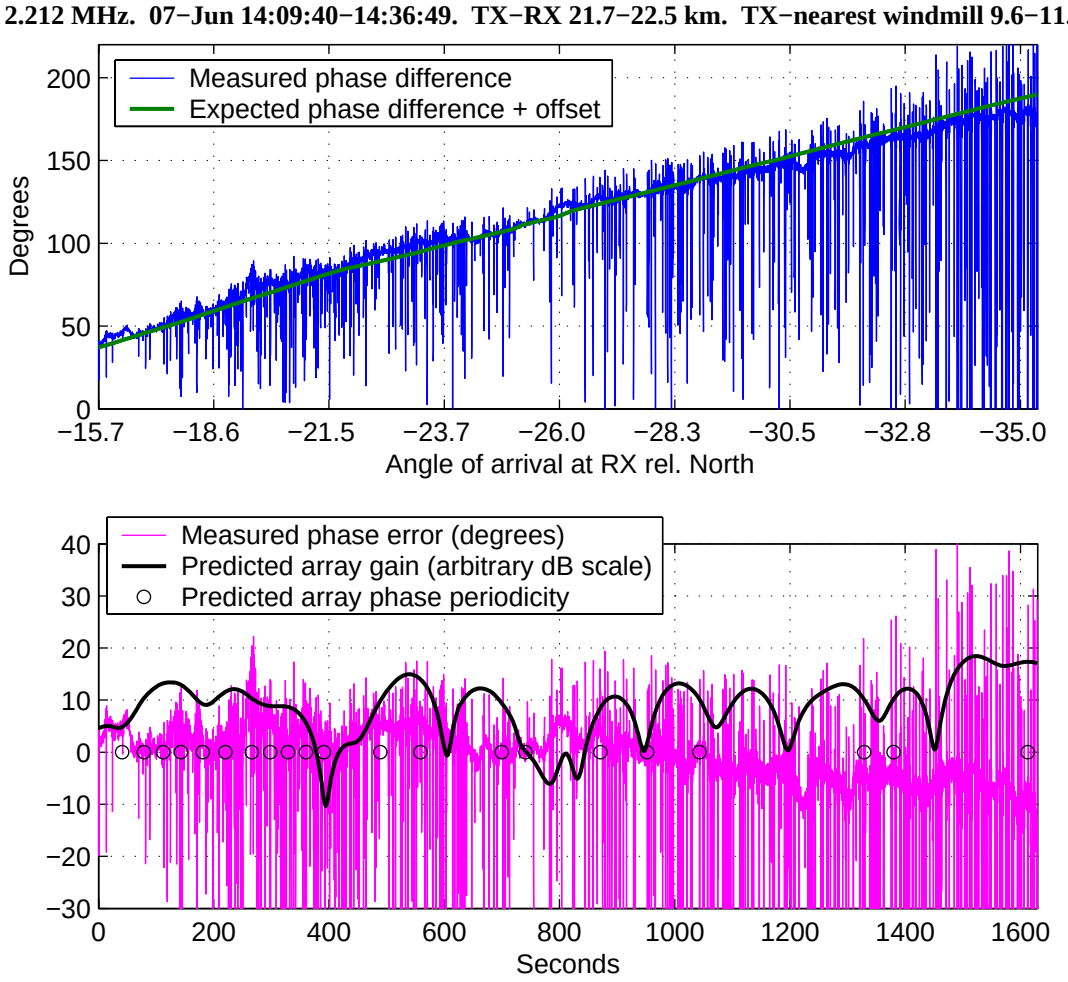

Figure 4.14 *Angular sweep at 2.212 MHz, transmitter North of Smøla far from shore (run 2). $k_{eff} = k/0.59$ is used to compute expected phase difference. See Sec. 4.13 for discussion on the large spikes in the measured phase difference.*

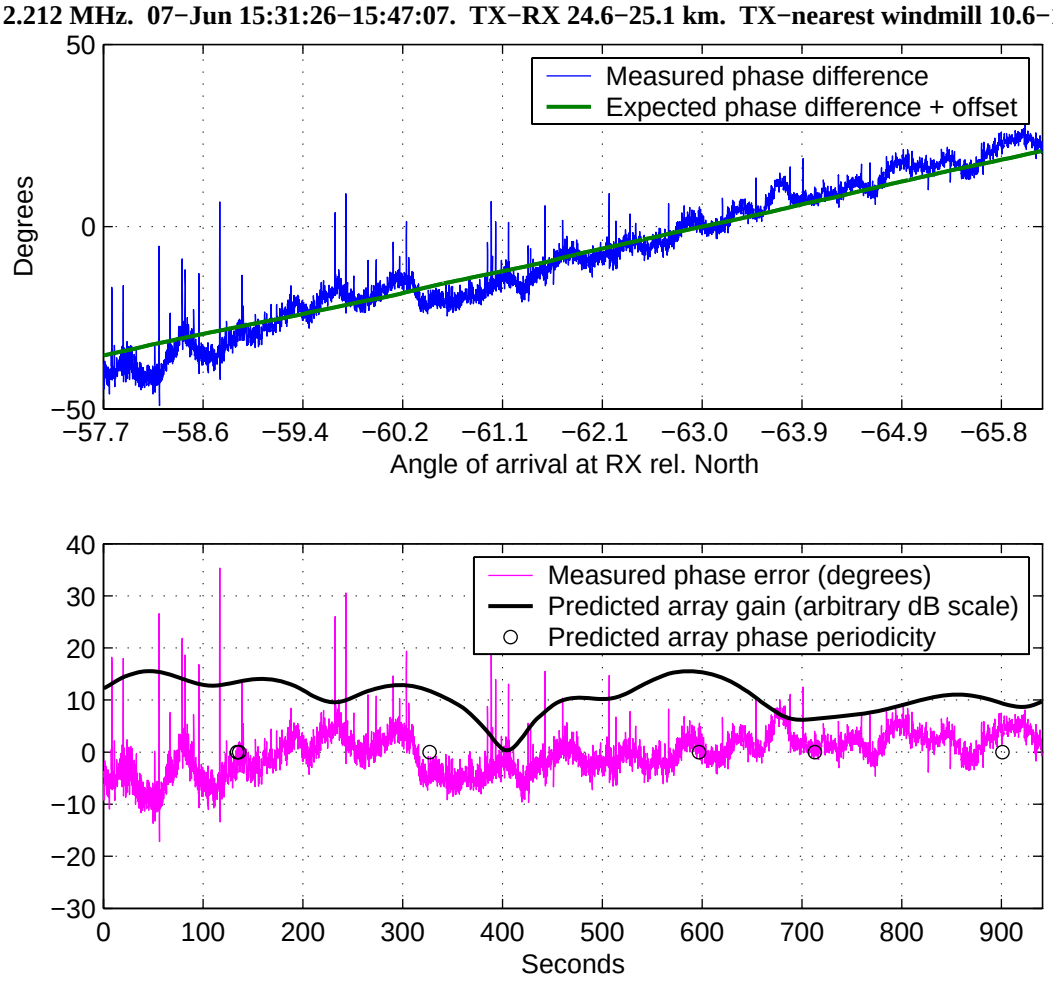

Figure 4.15 Angular sweep at 2.212 MHz, transmitter North of Smøla far from shore (run 2). $k_{eff} = k/0.59$ *is used to compute expected phase difference.*

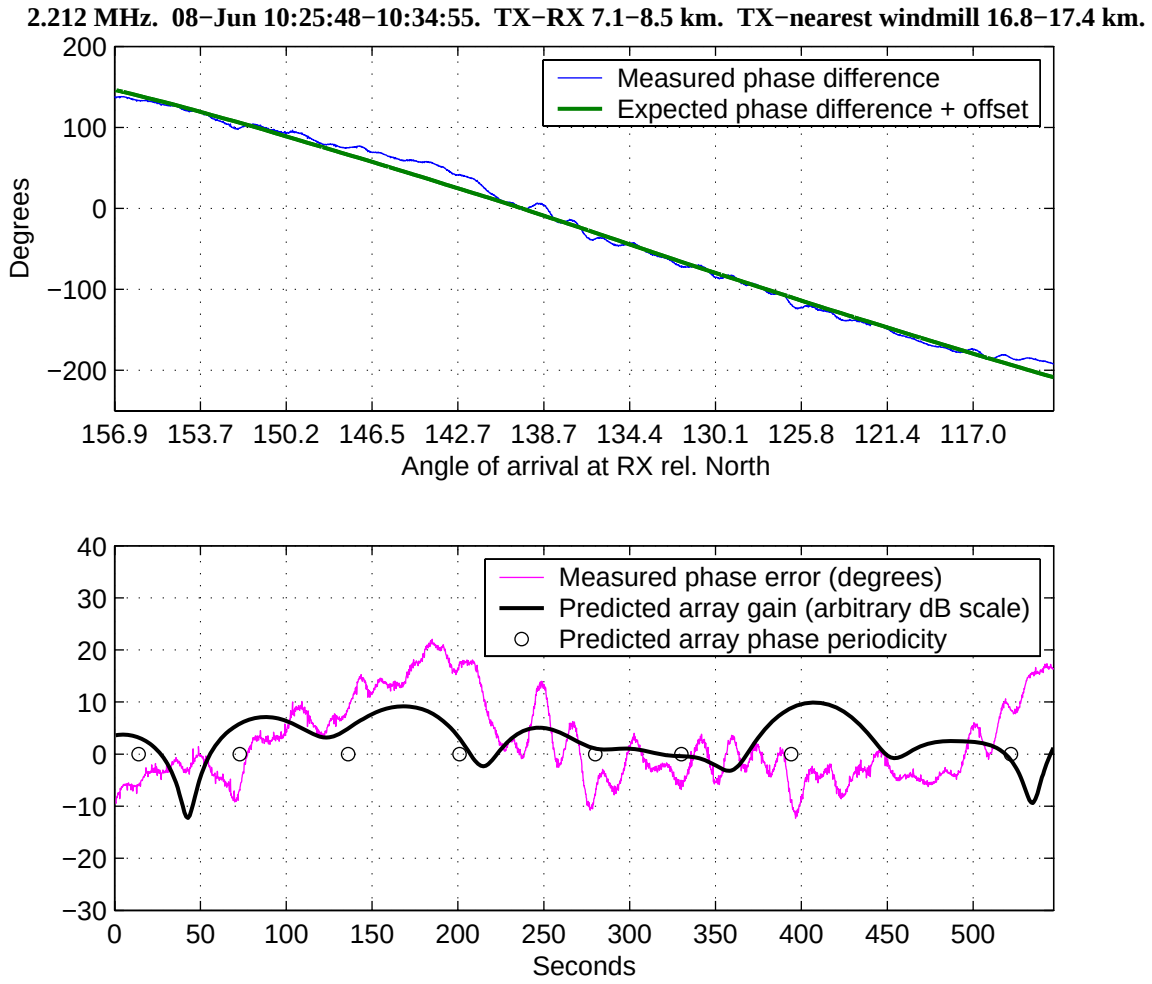

Figure 4.16 Angular sweep at 2.212 MHz, transmitter South of Smøla (run 5). $k_{eff} = k/0.59$ *is used to compute expected phase difference.*

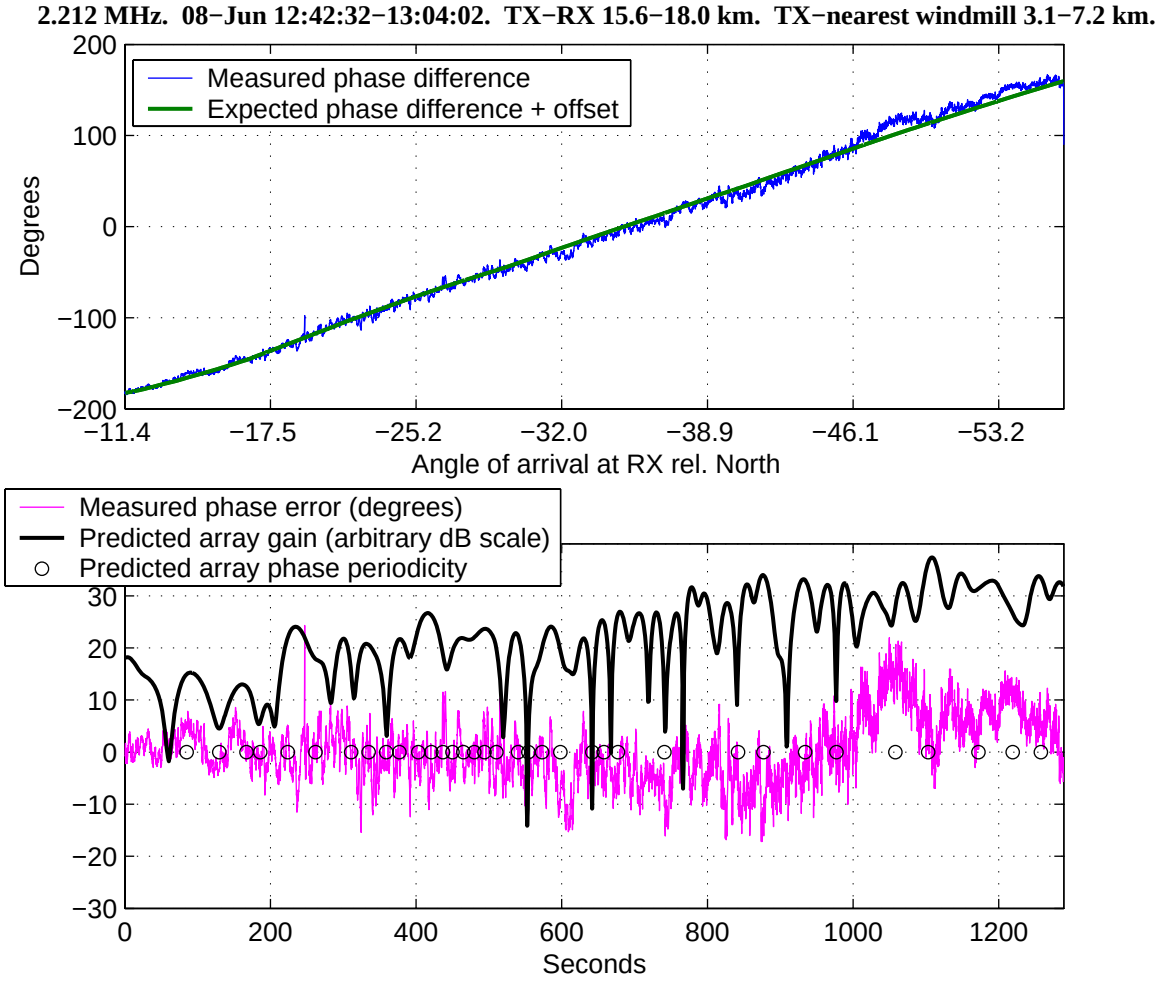

Figure 4.17 Angular sweep at 2.212 MHz, transmitter North of Smøla close to shore (run 7). $k_{eff} = k/0.59$ *is used to compute expected phase difference.*

4.12 Angular sweeps at 9.991 MHz

In Figs. 4.18-4.22 we also present measurements where the transmitter has performed angular sweeps with approximately constant TX-RX distance, with transmitter frequency of 9.991 MHz. In each figure, the upper and lower plots have identical time scales even though the upper plot is annotated by angle of arrival (AOA). Each figure spans a time interval where the AOA has been swept close to linearly and the measured phase difference does not wrap between ± 180 degrees. Note that the x-axes (time and angular scales) are different for the different figures.

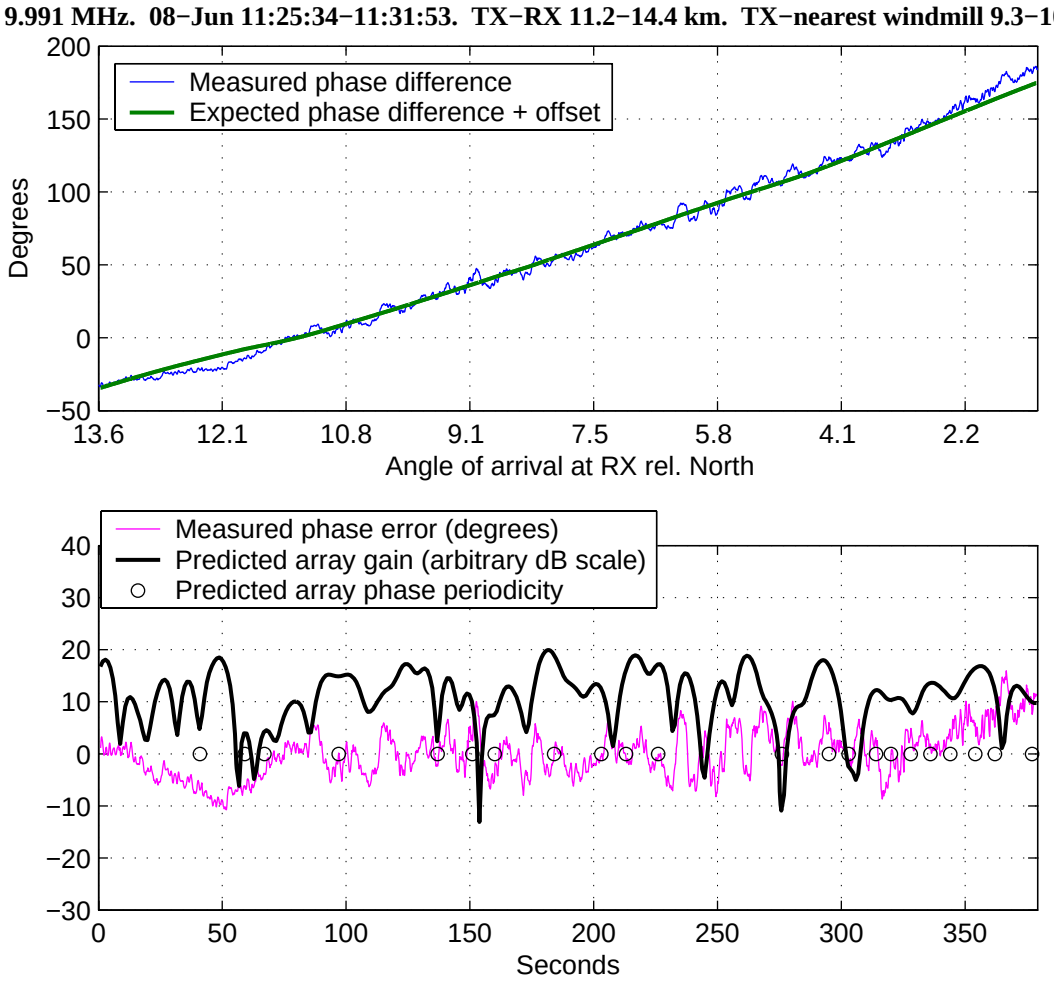

Figure 4.18 Angular sweep at 9.991 MHz, transmitter East of Smøla (run 6). $k_{eff} = k$ is used to compute expected phase difference.

At 9.991 MHz, the phase difference fluctuations when the transmitter is East of Smøla (Figs. 4.18-4.19) are in the range 5-15 degrees peak-to-peak. When the transmitter is North of Smøla and passes behind the wind farm close to shore (Figs. 4.20-4.22), the fluctuations are in the range 10-30 degrees peak-to-peak, and by visual inspection seem to be related to the predicted array factor. However, within the available time frame we were not able to find a mathematical relationship that would give clear statistical evidence of correlation between the predicted and measured phase fluctuations. This is not surprising, considering the number of idealizations in

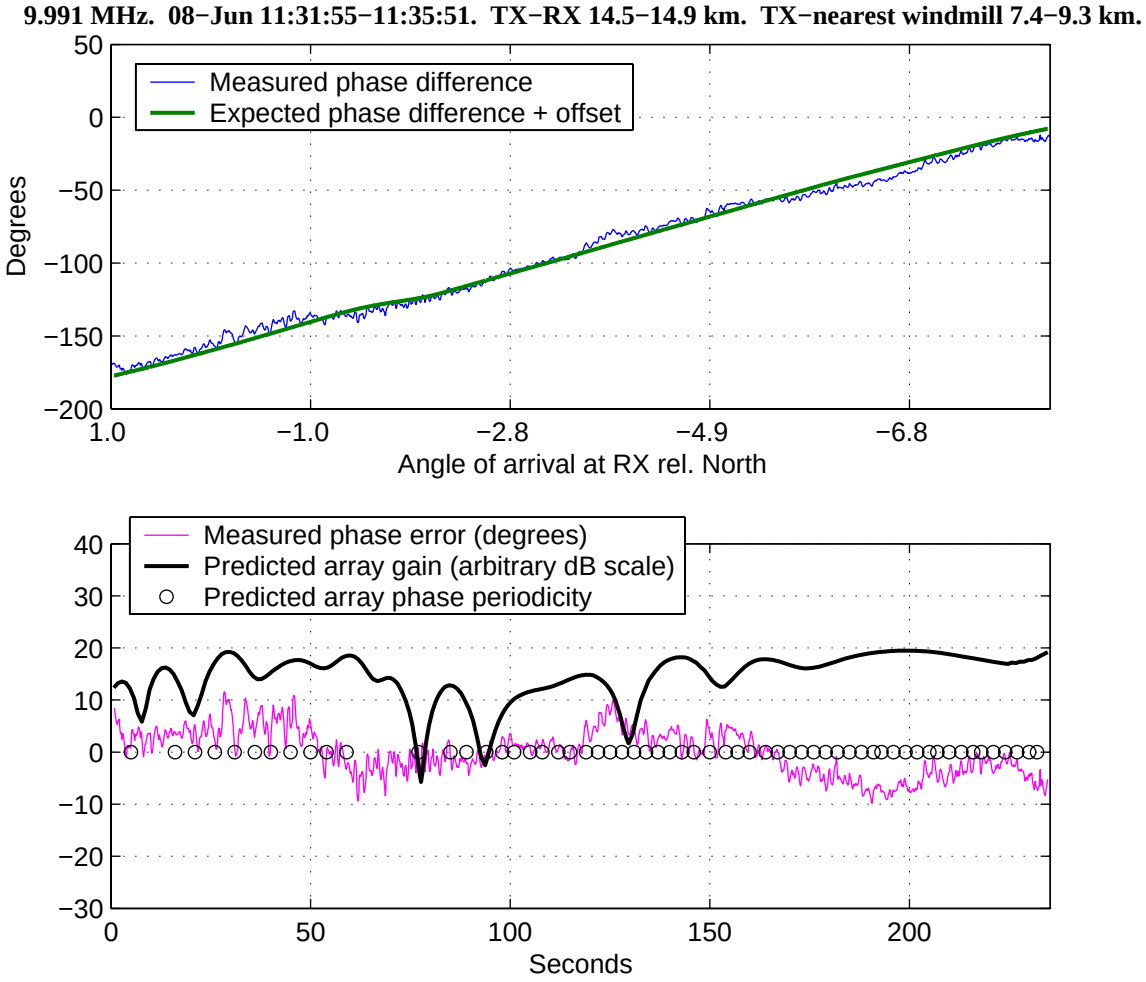

Figure 4.19 Angular sweep at 9.991 MHz, transmitter East of Smøla (run 6). $k_{eff} = k$ *is used to compute expected phase difference.*

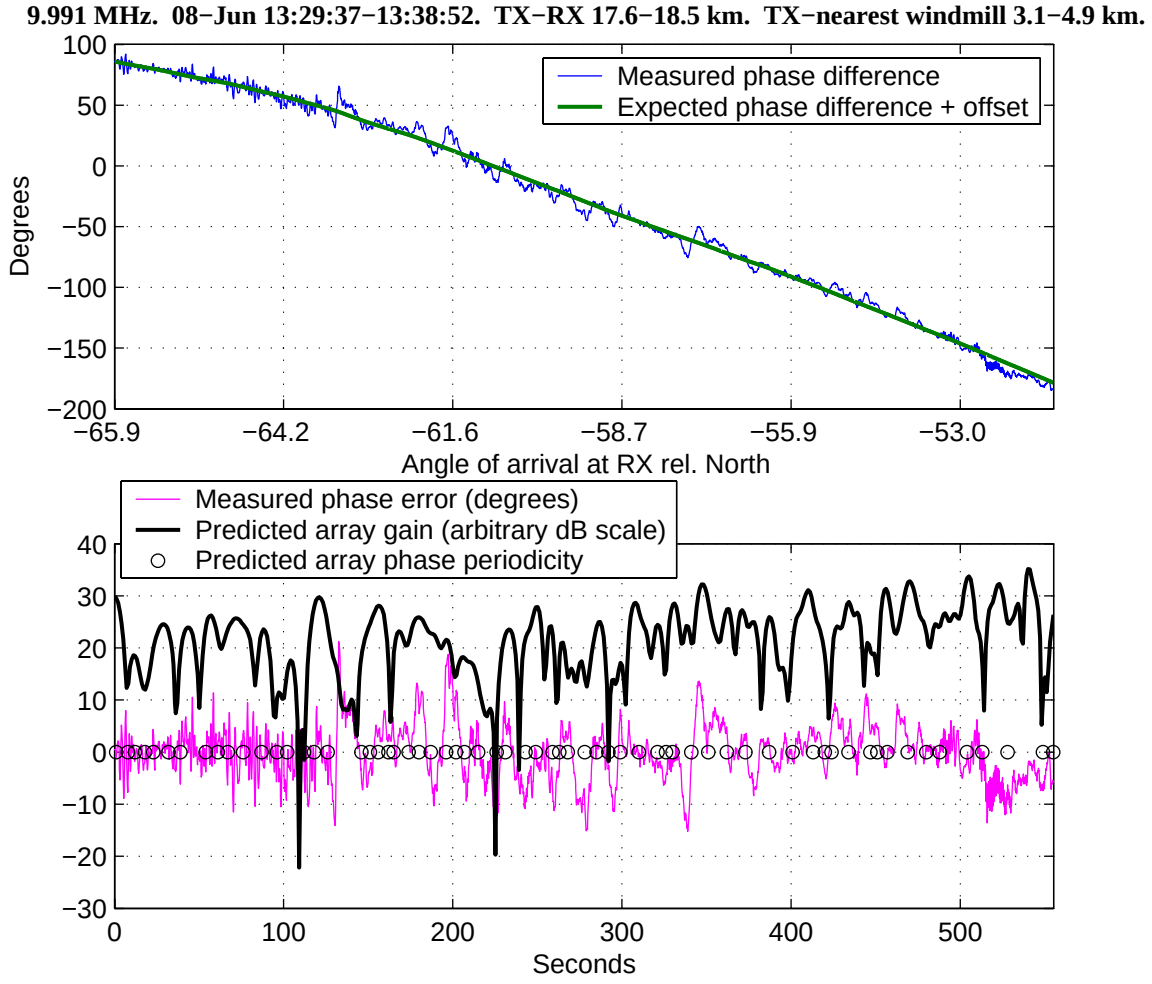

Figure 4.20 Angular sweep at 9.991 MHz, transmitter North of Smøla (run 8). $k_{eff} = k$ *is used to compute expected phase difference.*

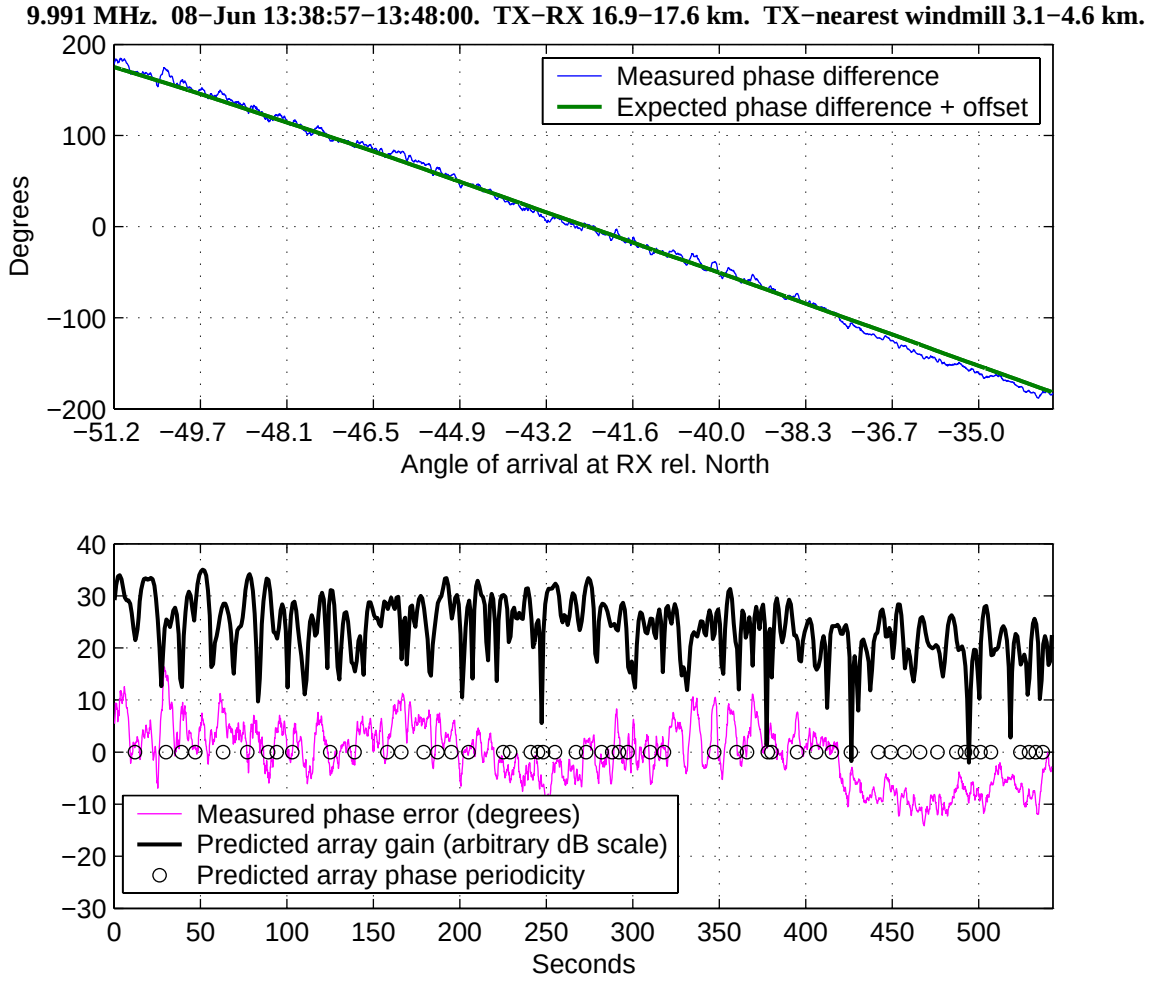

Figure 4.21 Angular sweep at 9.991 MHz, transmitter North of Smøla (run 8). $k_{eff} = k$ *is used to compute expected phase difference.*

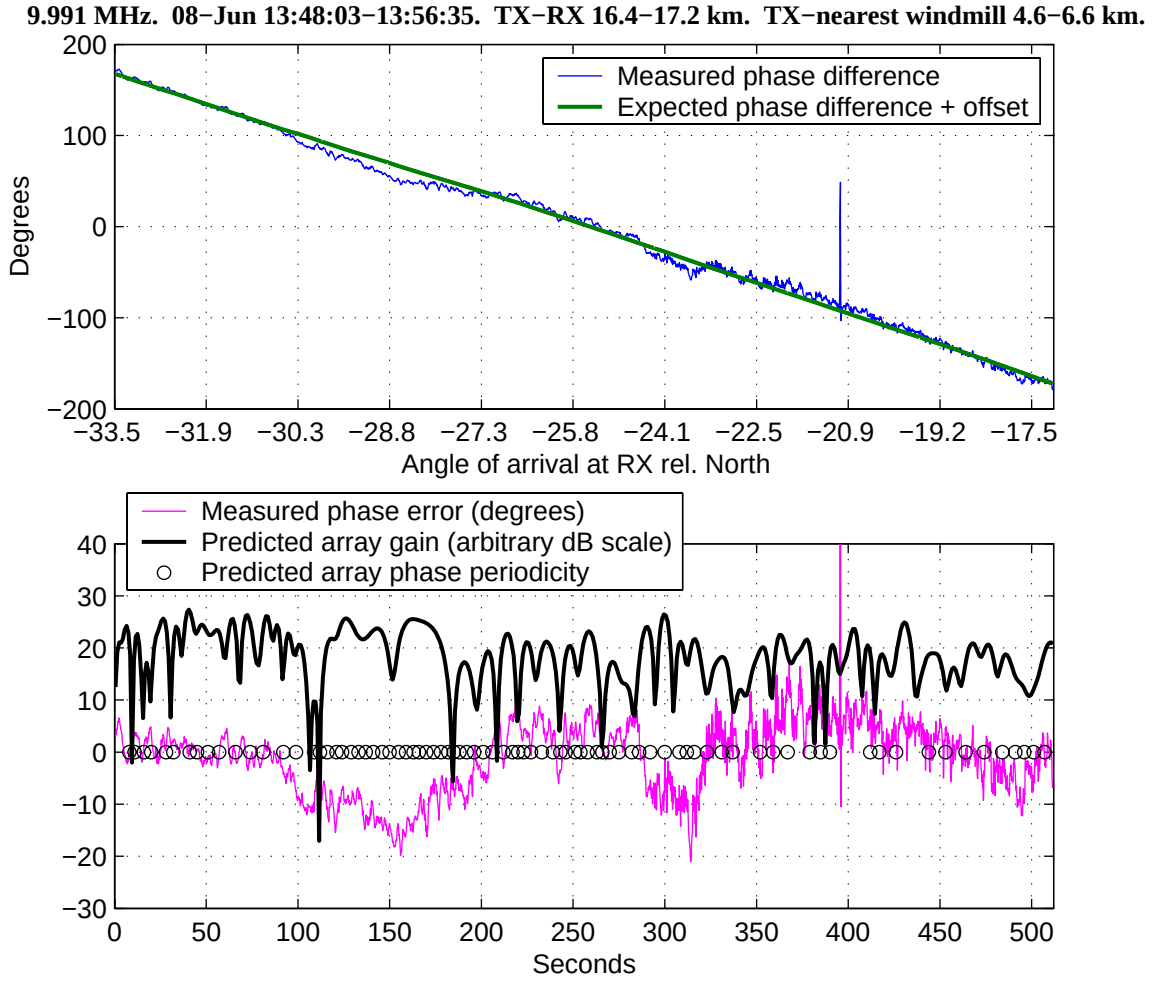

Figure 4.22 Angular sweep at 9.991 MHz, transmitter North of Smøla (run 8). $k_{eff} = k$ *is used to compute expected phase difference.*

the theoretical model.

To make a rough estimate of the bistatic radar cross section σ_N of the wind farm at 9.991 MHz, under the assumption that the fluctuations are really caused by scattering from the wind farm, we consider the phase fluctuations of 30 degrees peak-to-peak when the angle of arrival is about -62 degrees (Fig. 4.19). In order to cause fluctuations at this level, K_s in Eq. (3.3) must be approximately $\sin(30°/2) = 0.45 = -3.4$ dB. Evaluating the power budget as in Eq. (3.5), and taking into account the difference in transmission loss from the transmitter to the receiver relative to to the wind farm, we obtain the following rough estimate of σ_N:

$$\begin{aligned}
\sigma_N[\text{dBm}^2] &= 158.55\ \text{dBm}^2/\text{s}^2 \\
&\quad -140\text{dBHz}^2 \qquad 20\log_{10}(f) \\
&\quad -3.4\text{dB} \qquad K_s \\
&\quad +114.8\text{dB} \qquad L \text{ from wind farm to RX} \\
&\quad +95\text{dB} \qquad L \text{ from TX to wind farm} \\
&\quad -112.2\text{dB} \qquad L \text{ from TX to RX} \\
&= 112.8\text{dBm}^2
\end{aligned} \tag{4.2}$$

Here, the GRWAVE program[1] combined with Millington's method was used to predict the transmission loss from transmitter to receiver (1 km sea and 17 km land), from transmitter to centroid of wind farm (1 km sea and 6 km land), and from wind farm centroid to receiver (12 km land).

Note that this measurement-based estimate of σ_N is approximately 40 dB higher than what would be obtained by combining the prediction of σ_1 in Sec. 3.3 with the prediction of $|\chi|$ in Sec. 4.8, at 10 MHz. However, the estimate does not take into account the potential effect that shadowing by the wind farm may increase the path loss of the direct path (which would lead to a lower estimate of σ_N).

4.13 Extreme phase fluctuations at 2.212 MHz

Fig. 4.23 shows extreme phase fluctuations observed on Jun 7th at 15:00. Unfortunately, the immediate further history was not observed as the transmitter seized operating shortly after this, due to a loose connector.

In Fig. 4.24 is shown an FFT-based estimate of the power spectral density (PSD) of the phase fluctuations during the extreme event, as well as during a "normal" interval of the same length 42 minutes later. The PSD of the AGC voltage of one of the radios is also shown, to give an indication of the fluctuations caused by broadband noise from sheep fences. In both cases the PSDs were estimated over an interval of 2529 samples at a sampling rate of 10.627 Hz, and the Matlab commands issued to estimate the PSD were:

```
Nfft=1024;overlap=Nfft/2;fs=10.627;
psd(data,Nfft,fs,blackmanharris(Nfft),overlap,'linear');
```

[1]The following ground parameters were used in the GRWAVE predictions: Sea: $\sigma = 4$ S/m and $\epsilon_r = 70$. Land: $\sigma = 0.003$ S/m and $\epsilon_r = 22$

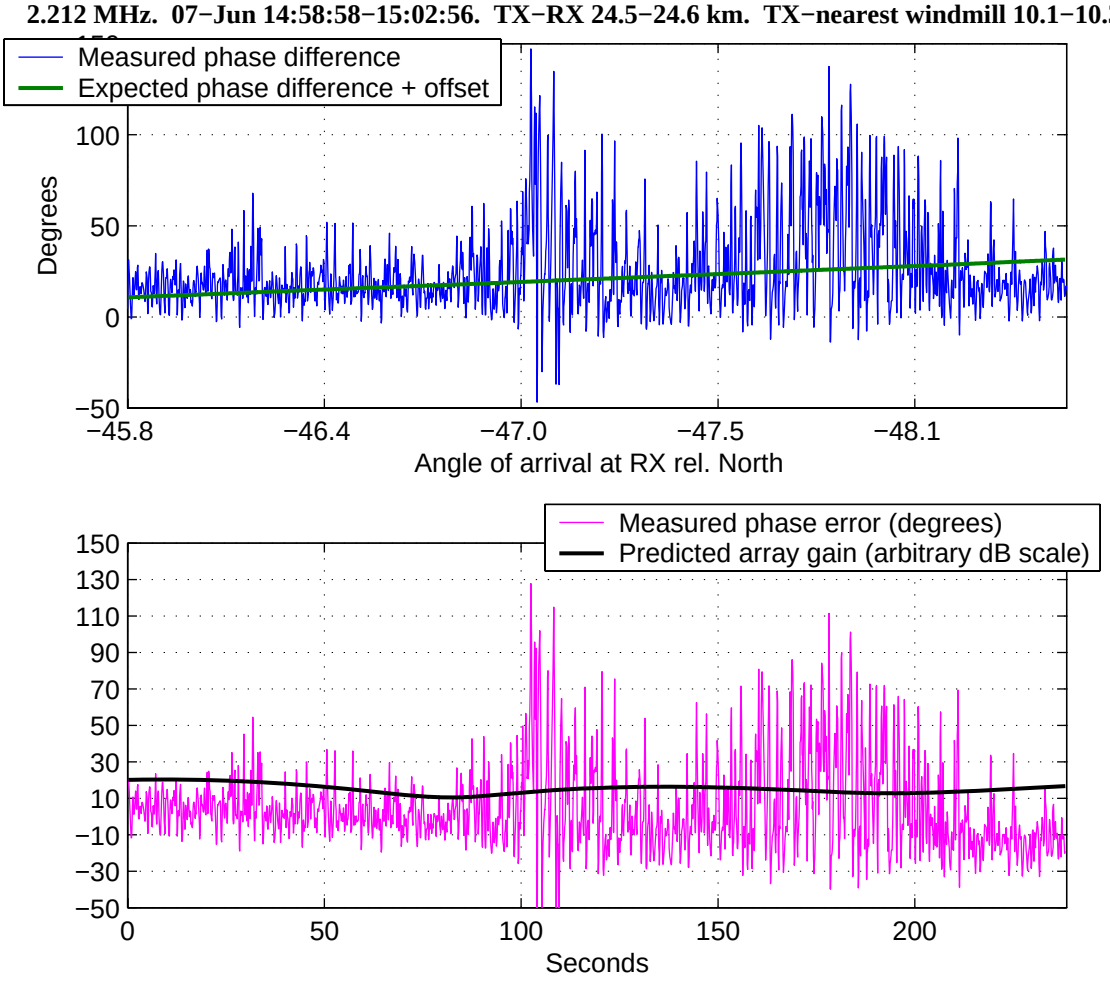

Figure 4.23 Extreme event observed at 2.212 MHz at Jun 7th (run 2), with TX behind wind farm as seen from RX.

Phase deviations of the same scale were observed also on June 6th, when the transmitter was in exactly the same position and further West, as shown in Fig. 4.25. At this time, phase difference measurements were logged manually every 10 seconds, and the integration time of the phase difference meter was about 3 seconds in order to ease the manual logging. Hence, fine-scale time fluctuations were not observed. However, these observations strongly suggest that the extreme event shown in Fig. 4.23 was not incidental.

Fig. 4.26 shows measurements when the transmitter was operational again, after the extreme event on Jun 7th (note that part of this time interval is also shown in Fig. 4.15). The extreme phase deviations in the first part of this plot are not coherent with the noise from sheep fences (as observed in the AGC voltage). The estimated PSDs with and without extreme phase deviations are shown in Fig. 4.27.

As seen in Fig. 4.14, extreme phase deviations were also present earlier in the run, and increasing in amplitude as the transmitter approached to the point in Fig. 4.23. These were neither coherent with the sheep fences.

The power spectra show that the fluctuations are broadband in nature, but have small peaks at

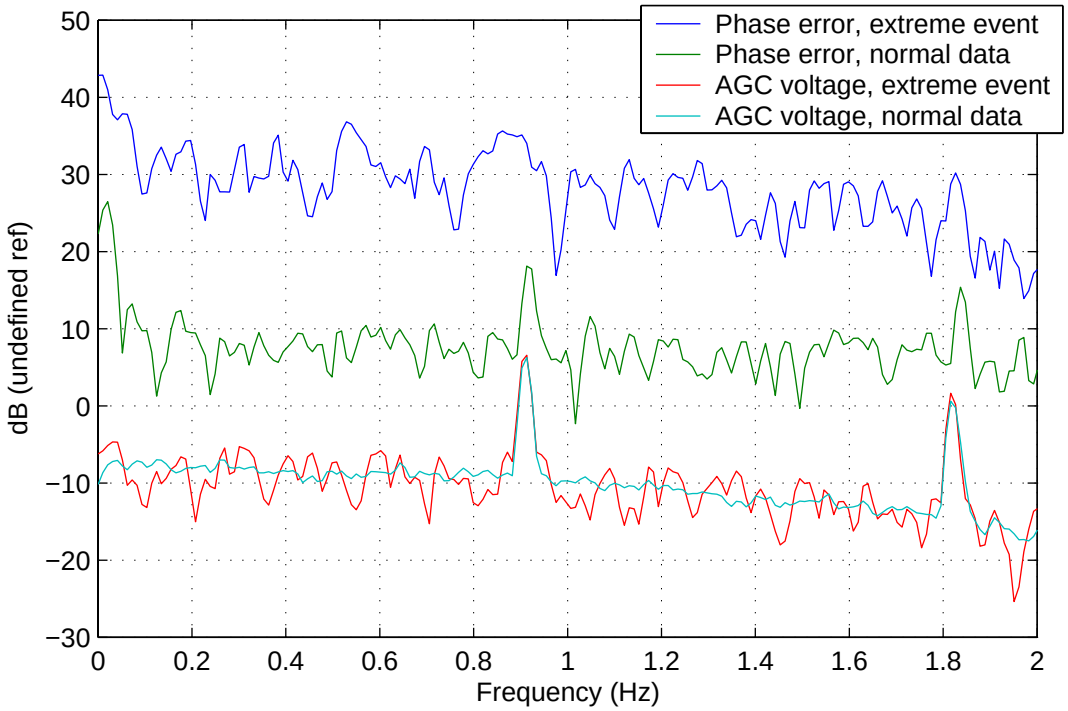

Figure 4.24 Estimated power spectral density of phase fluctuations and AGC voltage during extreme event on Jun 7th, and 42 minutes later ("normal data").

the blade frequencies of about 0.55 Hz and 0.85 Hz. This, in combination with the fact that the fluctuations are only seen when the transmitter is behind the wind farm, provides an indication that the fluctuations are related to the blade rotation of the wind turbines.

The extreme phase fluctuations are mainly observed when the wind farm is in the direct path between transmitter and receiver. This suggests that they may be related to shadowing effects in combination with blade rotation, and we have two hypotheses to explain the observed phenomena (isolated or in combination):

1. (Hypothesis) Shadowing causes increased path loss in the direct path, increasing the importance of the scattered paths. The operating frequency is close to the resonant frequency of the wind turbines, and the resonant scattering of each wind turbine is modulated by the blade rotation. The resulting variations in scattered signal amplitude will give rise to observed phase fluctuations.

2. (Hypothesis) Shadowing effects on the direct wave are modulated by the blade rotation due to resonance. Scattered paths will dominate more or less depending on this modulation, causing phase fluctuations.

This kind of fluctuations was not observed when the transmitter was in the same relative angle to the wind farm, but closer to shore (Fig. 4.17). This does not counter the hypothesis that the extreme fluctuations may be related to the wind farm, since (a) with the transmitter closer to shore the signal would arrive different wind turbines at different angles, such that coherent addition of a resonant scattering phenomena would be less likely, and (b) this was at a different day, when the wind turbines may have been pointing in a different direction.

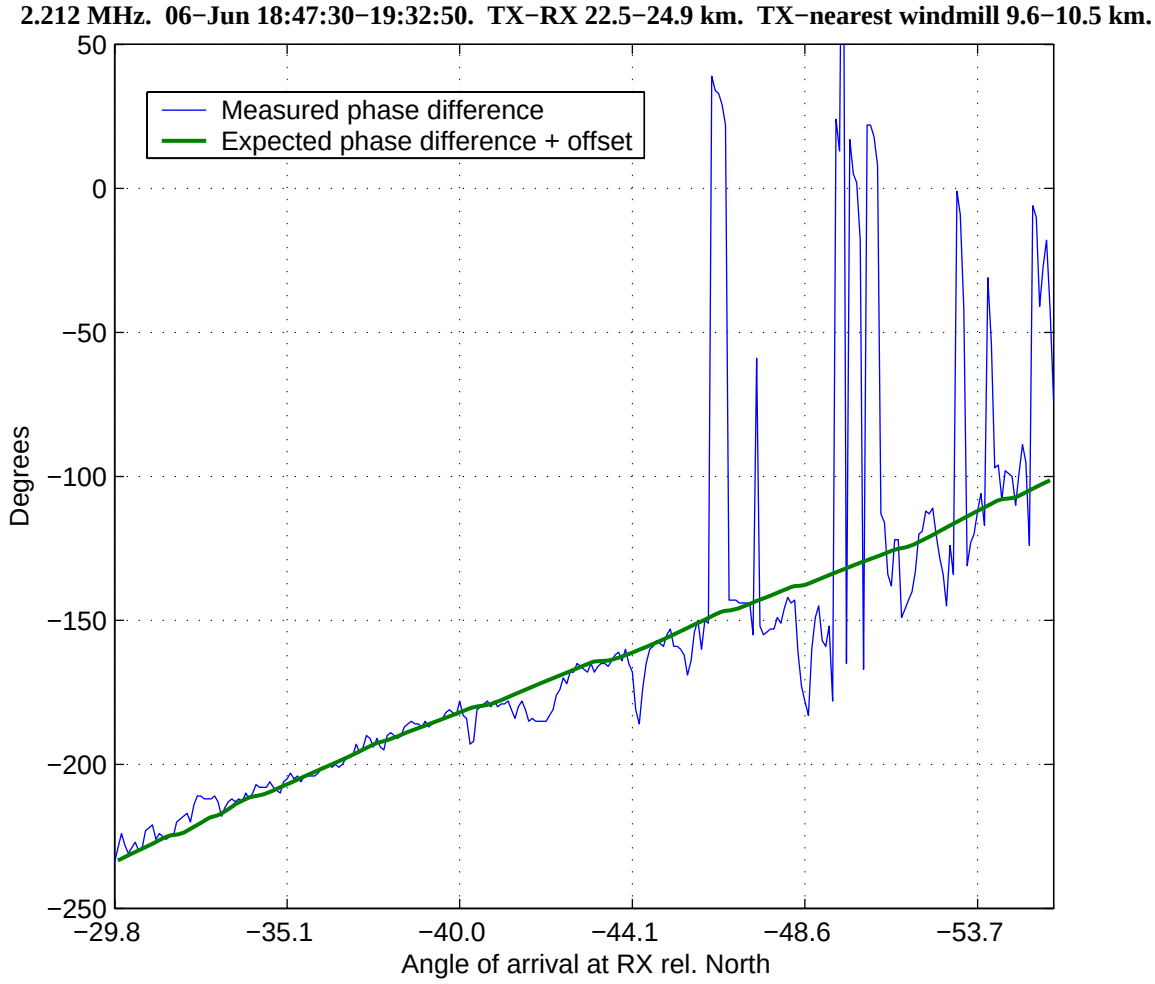

Figure 4.25 Extreme event observed at 2.212 MHz at Jun 6th (run 1), with TX behind wind farm as seen from RX. Manually logged measurements every 10 seconds.

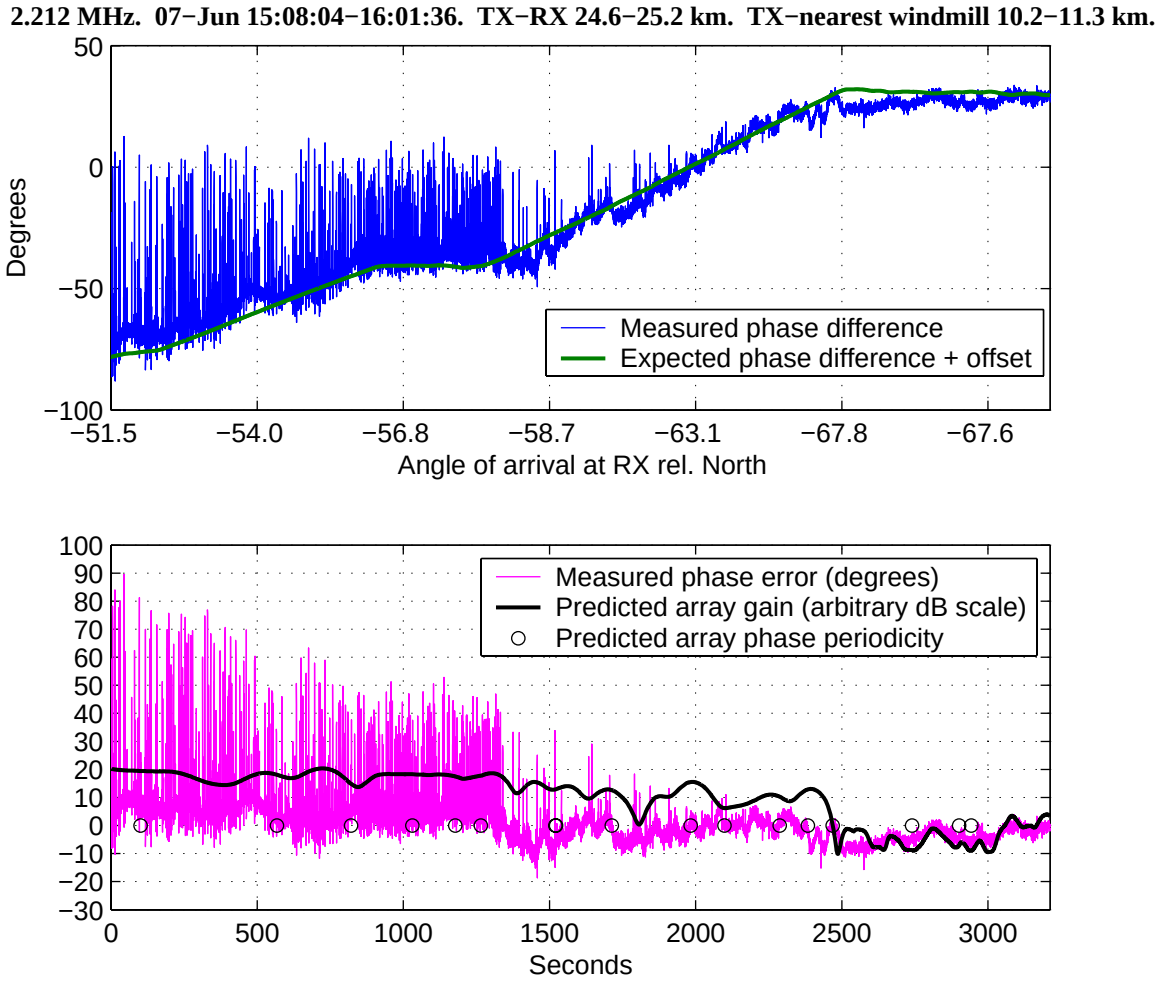

Figure 4.26 Observations after extreme event on Jun 7th, with TX further West (run 2).

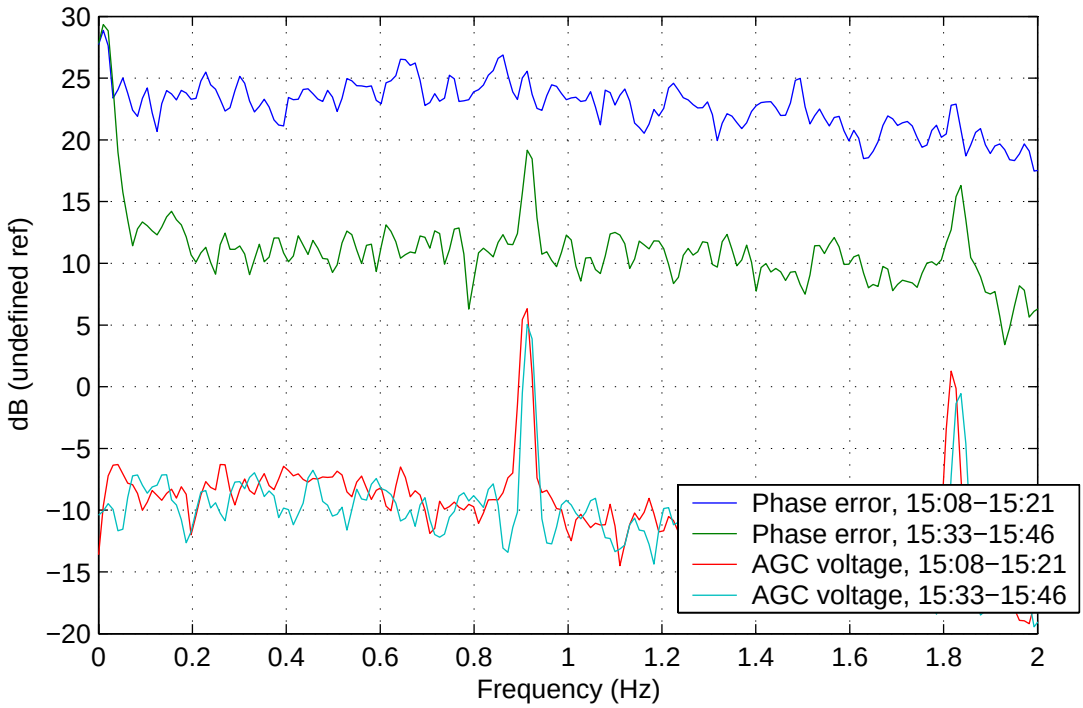

Figure 4.27 Estimated power spectral density of phase fluctuations and AGC voltage during two different time intervals in Fig. 4.26.

There is also a possibility that the extreme fluctuations are due to equipment malfunction (considering that the transmitter seized to operate twice during run 2), due to low signal levels (the fluctuations were observed in the area of maximum TX-RX distance), or caused by interference not observable in the AGC voltage. The first and third of these possible explanations are partly countered by the similar observation in Fig. 4.25.

To cause phase fluctuations of about 100 degrees as observed here, the scattered signal must be approximately equally strong as the direct signal, $K_s = 0$ dB. Using the same method as in Sec. 4.12 above (transmitter to receiver path is 8 km sea and 16 km land, transmitter to centroid of wind farm is 7 km sea and 5 km land), we obtain the following rough estimate for σ_N.

$$\begin{aligned} \sigma_N[\text{dBm}^2] &= 158.55\ \text{dBm}^2/\text{s}^2 \\ &\quad -126.9\text{dBHz}^2 \quad 20\log_{10}(f) \\ &\quad -0\text{dB} \quad K_s \\ &\quad +84.4\text{dB} \quad L \text{ from wind farm to RX} \\ &\quad +71.3\text{dB} \quad L \text{ from TX to wind farm} \\ &\quad -85.4\text{dB} \quad L \text{ from TX to RX} \\ &= 102.0\text{dBm}^2 \end{aligned} \tag{4.3}$$

Note that this measurement-based estimate of σ_N is approximately 20 dB higher than what would be obtained by combining the prediction of σ_1 in Sec. 3.3, assuming resonant scattering, with the prediction of $|\chi|$ in Sec. 4.8, at 2 MHz. However, the estimate does not take into account the potential effect that shadowing by the wind farm may increase the path loss of the direct path (which would lead to a lower estimate of σ_N).

4.14 Other measurements

For completeness, we also include plots of the measurements not discussed previously.

In Fig. 4.28 is shown measurements where the transmitter movement was mainly in the radial direction relative to the receiver, at 2.833 MHz. The upper and lower plots have identical time scales even though the upper plot is annotated by TX-RX distance. In Fig. 4.29 is shown an angular sweep at 2.833 MHz.

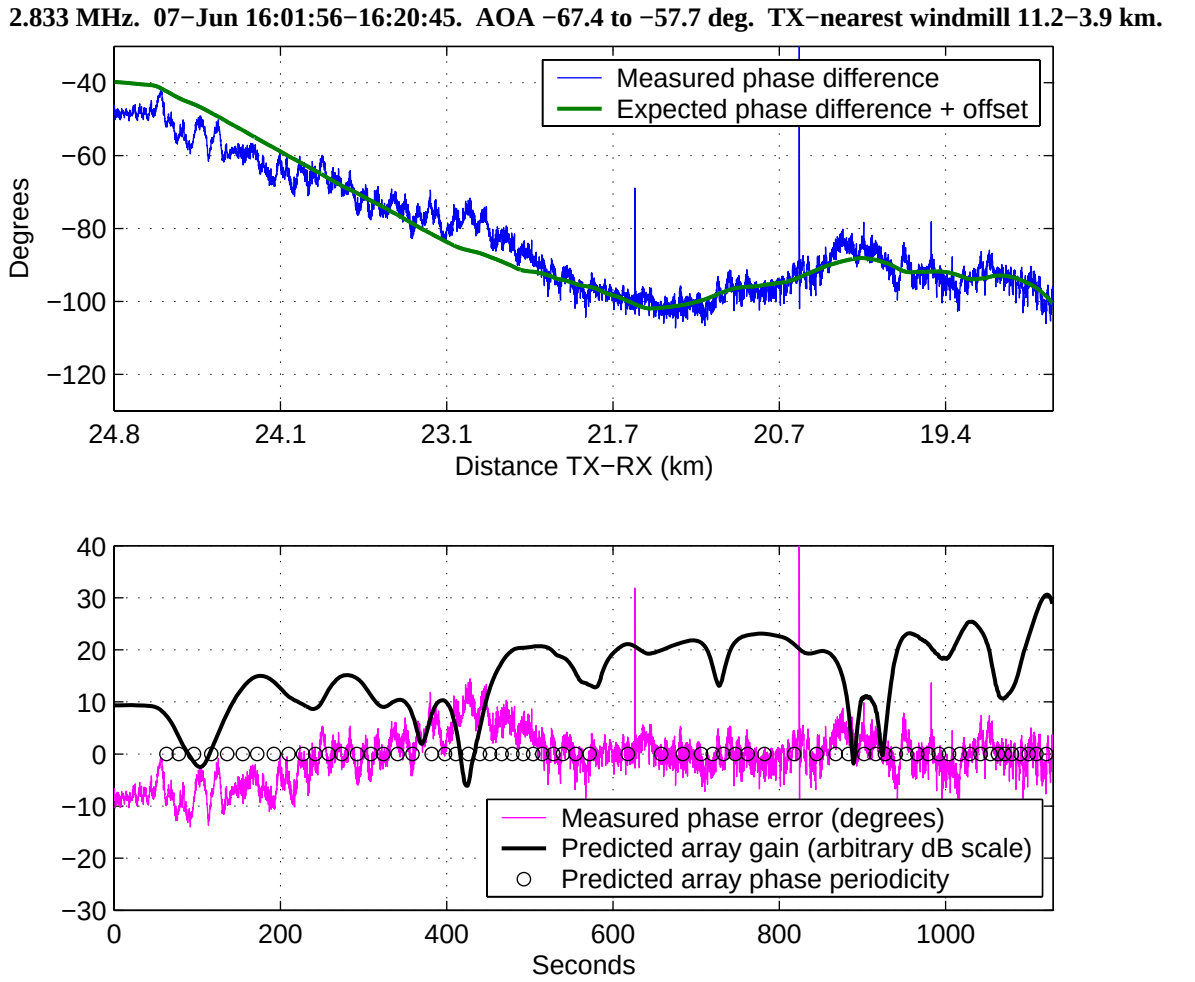

Figure 4.28 Radial sweep at 2.833 MHz, transmitter North of Smøla (run 3). $k_{eff} = k/0.775$ *is used to compute expected phase difference.*

In Figs. 4.30-4.31 are shown the measurements at 2.212 MHz while the boat was operating East of Smøla and filling gas. Note that there are some large errors in the predicted phase difference. This is probably due to the the calibration factor η varying with angle of arrival when the signal enters from the East, along the shore.

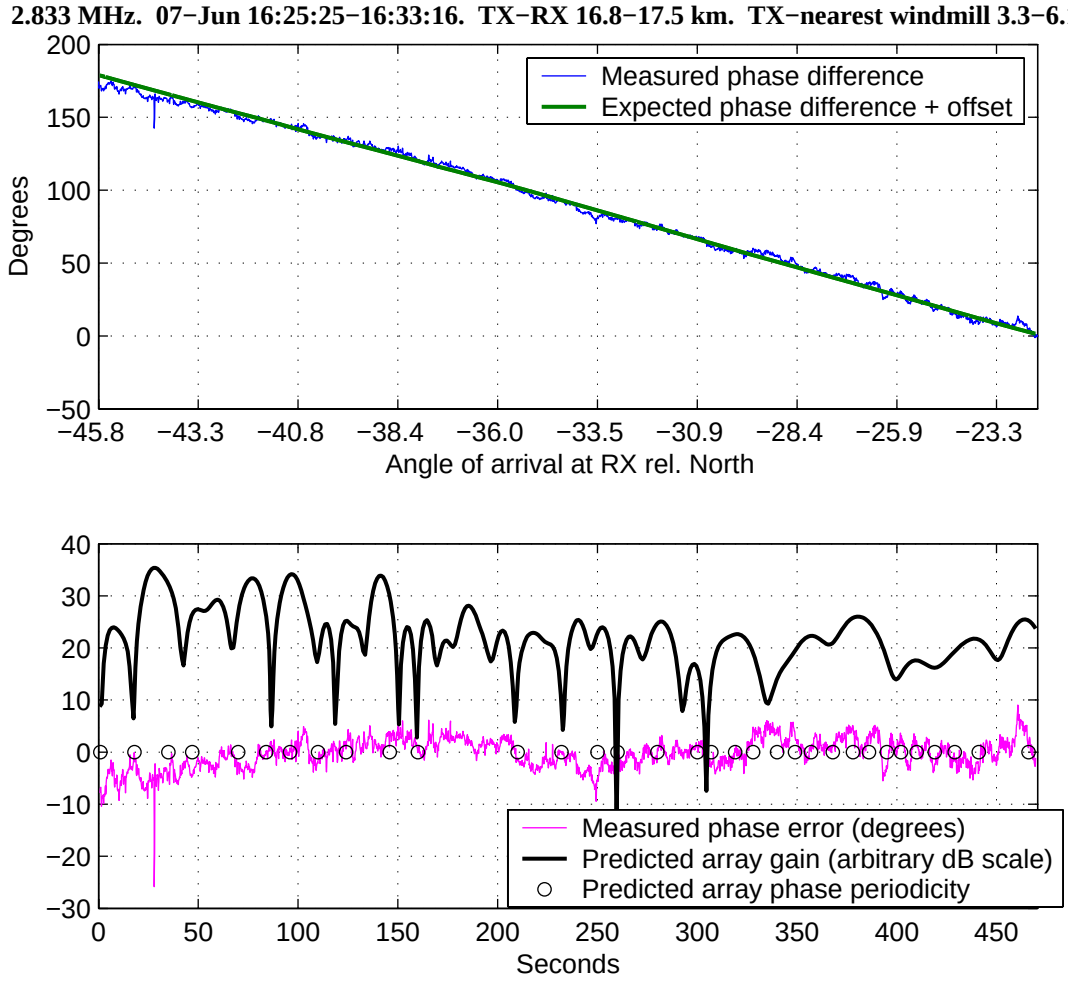

Figure 4.29 Angular sweep at 2.833 MHz, transmitter North of Smøla (run 3). $k_{eff} = k/0.775$ *is used to compute expected phase difference.*

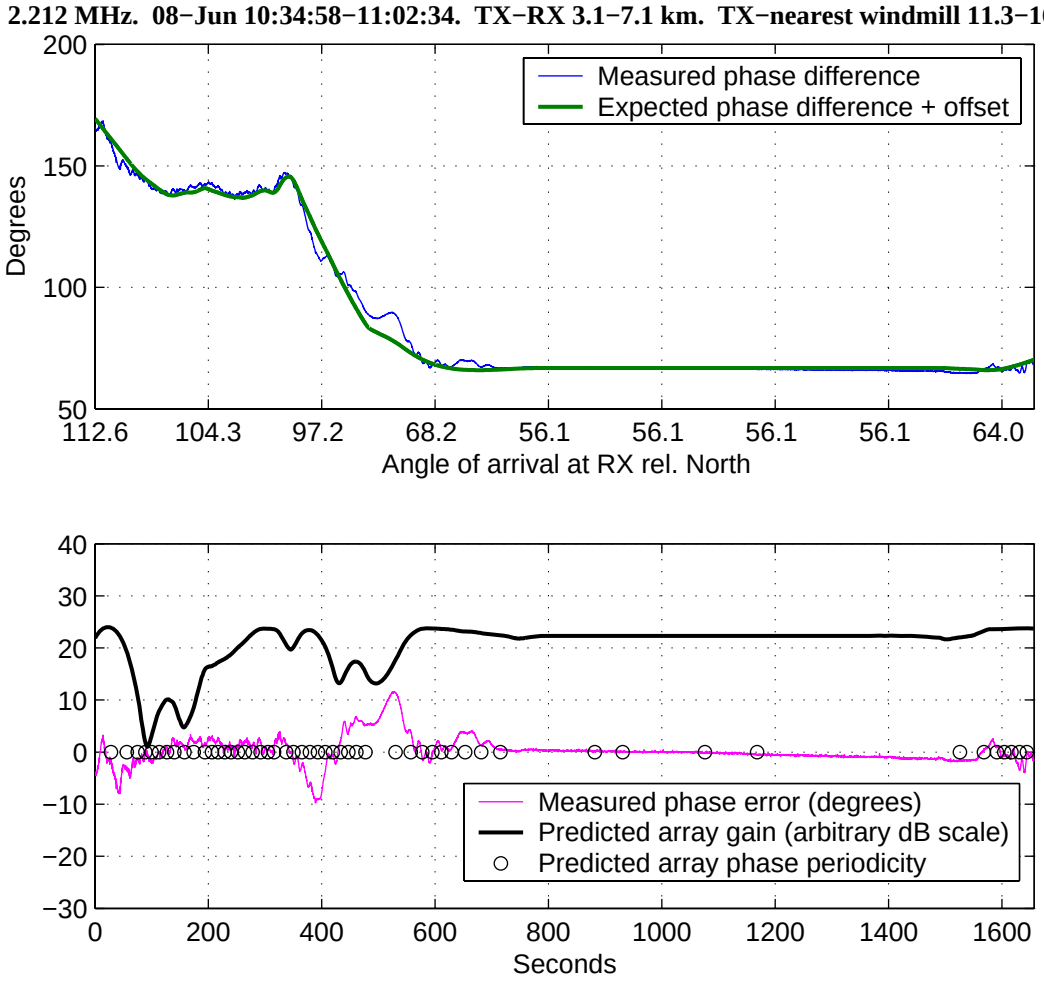

Figure 4.30 Measurements at 2.212 MHz, transmitter East of Smøla and stopping for gas (run 5). $k_{eff} = k/0.98$ is used to compute expected phase difference.

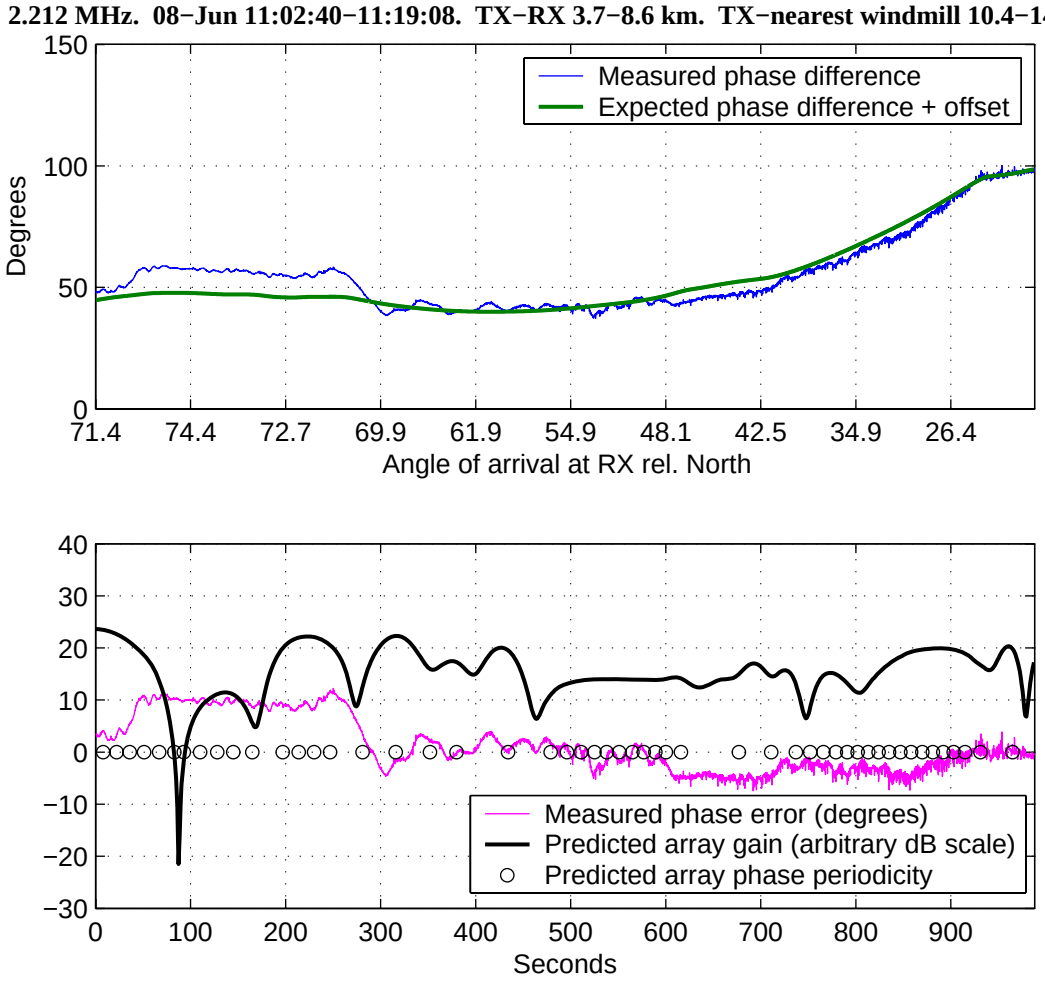

Figure 4.31 Measurements at 2.212 MHz, transmitter East of Smøla close to shore (run 5). $k_{eff} = k/0.98$ is used to compute expected phase difference.

4.15 Summarizing discussion

4.15.1 General observations

The main observations at the frequencies 2.212 and 9.991 MHz are summarized in Figs. 4.32-4.33. The measurements at 2.833 MHz are not discussed further here due to their limited extent.

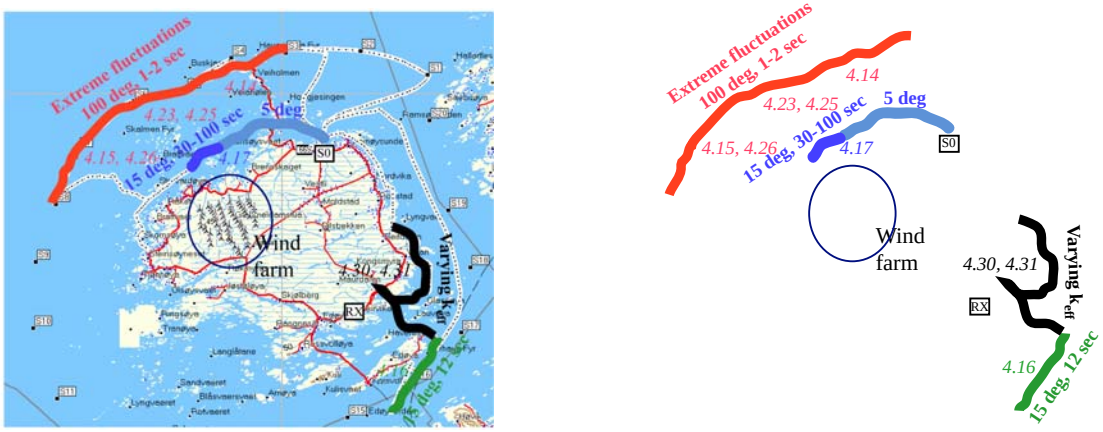

Figure 4.32 *Summarizing figure for measurements at 2.212 MHz. With (left) and without (right) map overlay. Boldface comments refer to phase fluctuations (in units of electrical phase difference), while italics refer to figure numbers in this report.*

Figure 4.33 *Summarizing figure for measurements at 9.991 MHz. With (left) and without (right) map overlay. Boldface comments refer to phase fluctuations (in units of electrical phase difference), while italics refer to figure numbers in this report.*

At 2.212 MHz, we make the following observations (the relationship between angle of arrival α and electrical phase difference ϕ at broadside is $\alpha = \phi/7.85$, assuming $\eta = 0.59$):

- The interferometer has to be calibrated by setting $k_{eff} = k/\eta$, where the calibration factor η is equal to 0.59 when the transmitter was North or South of Smøla. This is probably due to reflections from the land-sea boundary close to the interferometer.

- When the transmitter is South of Smøla, there are phase fluctuations of about 15 degrees with periodicity corresponding to about 1 degree in AOA (see Fig. 4.16). Possible explanations for these fluctuations are **(a)** small-scale variations in the calibration factor η due to local ground conditions near the land-sea boundary (but theoretically, such variations should be on a larger angular scale), **(b)** scattering from the wind farm, or **(c)** natural scattering effects from the mountains on the other side of the fiord. Path loss predictions with the transmitter South of Smøla shows that the total path loss transmitter-mountains-receiver is approximately 30 dB lower than the total path loss transmitter-wind farm-receiver. Thus, the scattering strength of the wind farm would need to be at least 30 dB higher than that of the mountains for scattering from the wind farm to dominate over mountains. To verify whether this is realistic would require exact numerical modelling of scattering from the mountains as well as from the wind farm, which there has not been time for in the present study.

- When the transmitter is North of Smøla close to shore, the phase fluctuations are stronger when the transmitter is behind the wind farm as seen from the receiver, compared to when it is further East (see Fig. 4.17). When behind the wind farm, the phase fluctuations are about 15 degrees with periodicity corresponding to 1-3,6 degrees in AOA. It seems probable, but not certain, that these fluctuations are due to scattering from the wind farm. In this geometry, scattering from mountains is less likely than when the transmitter is South of Smøla.

- When the transmitter is North of Smøla far from shore, extreme phase fluctuations of up to about 100 degrees are observed when the transmitter is behind the wind farm (see Sec. 4.13). The time scales of the fluctuations are in the same range as the wind turbine blade rotation. These fluctuations may be due to shadowing and/or scattering effects modulated by the blade rotation.

- When the transmitter is East of Smøla, it is near the endfire direction where the sensitivity of the interferometer is decreased. The signal also arrives along the shore such that variations in η are likely by geometrical considerations. For these data, it has not been possible to find a constant value of η that gives good calibration (see Figs. 4.30-4.31)

At 9.991 MHz, we make the following observations (the relationship between angle of arrival α and electrical phase difference ϕ at broadside is $\alpha = \phi/20.9$, assuming $\eta = 1$):

- Interferometer calibration is not needed; the measured phase differences seem plausible with $k_{eff} = k$ ($\eta = 1$).

- When the transmitter is East of Smøla, the phase fluctuations are in the range of 5-15 degrees (see Figs. 4.18-4.19).

- When the transmitter is North of Smøla, the fluctuations are in the range of 10-30 degrees, and most evident when the transmitter is behind the wind farm (see Figs. 4.20-4.22). Also, the time scale of the fluctuations is similar to that predicted by the "array factor" computed by considering a single scatterer at each wind turbine location

(see Sec. 4.8). The observed fluctuations are therefore likely to be due to scattering from the wind farm.

It should be noted that even though the measurement equipment gives a good indication of phase fluctuations, it is not able to measure absolute phase difference. Hence, any bias in the phase difference over a large angular sector would not be captured by the measurement setup.

4.15.2 In-depth analysis

In summary, the following hypotheses have been tested:

1. The wind farm generates a specific predictable signature based on the interaction of the wind turbine towers with the electromagnetic field. This is recognized as a specific response for phase variations vs angle as predicted by theoretical modelling. This phenomenon is readily identifiable where it is dominant, and is recognized through the scale and pattern of variations, allowing for translation in interference nulls and phases of scale components.
2. There is a natural background of influences from scattering from the terrain. This is expected to be stable and with medium to large scale variations vs angle as given by the range to the local terrain. Typically these fluctuations are expected to contain a number of different scales due to the varying size of terrain features, as described in Sec. 4.9 (in good agreement with e.g. Fig. 4.14).
3. The wind farm generates rapid fluctuations due to the motion of the blades, which generates pseudorandom signatures. This is a phenomenon which has been included due to the obvious existence of these phenomena in the observed data. The rapid fluctuations of these can not be explained by spatial interference, and are thus spatio-temporal effects where the rotation of the blades gives rapid and random changes. Overall this effect may be coexistent with phenomena 1.

These hypotheses are manifested as an RMS variation in phase supported by the characteristics in response vs angle. In a full-blown setup this can rigorously be measured. As the current setup is manually calibrated, these variations can best be assessed using a combination of actual measurements and engineering judgment. These assessments are summarized in Table 4.4. One should be aware of the possibility that natural variations have been mistaken as wind farm fingerprint, and/or that fluctuations due to the wind farm have been mistaken as natural variations. This may e.g. have happened if some unknown important aspect of the wind farm scattering has not been taken into account by the theoretical model.

The overall findings are as follows:

- Maximum wind farm fingerprint behind wind farm is $10^\circ \pm 3^\circ$ RMS phase fluctuation at expected resonance frequency (2.212 MHz). The value at 2.833 MHz is lower, but due to limited amount of data, no specific range of values can be set. At 9.991 MHz, the levels are estimated at $6^\circ \pm 3^\circ$.

Frequency	**Angular data**		**Measurement overview**			**Observation**	
MHz	from North °	from edge wind farm °	Phenomenon 1 Wind farm fingerprint RMS phase	Phenomenon 2 Terrain signature RMS phase	Phenomenon 3 Wind farm rotor Peak phase	Date	Start time
2.212	-65	5	1	**3**	**5**	June 7	153126
2.212	-63	3	**4**	<1	**6**	June 7	150804
2.212	**-58**	**0**	**4**	***4***	**40**	June 7	153126
2.212	**-52**	**0**	**5**	***4***	**70**	June 7	150804
2.212	**-50**	**0**	**10**	5	**<2**	June 8	124232
2.212	**-48**	**0**	**10**	<5	**170**	June 6	184730
2.212	**-47**	**0**	**10**	<5	**160**	June 7	145858
2.212	-35	5	***<5***	**5**	**unknown**	June 6	184730
2.212	-35	5	***2***	**3**	**200**	June 7	140940
2.212	-20	20	***2***	**3**	**40**	June 7	140940
2.212	-20	20	<3	**5**	<2	June 8	124232
2.212	30	50	<2	**2**	<4	June 8	110240
2.212	140	180	<10	**10**	<1	June 8	102548
9.991	-65	5	<2	**3**	<1	June 8	122937
9.991	**-55**	**0**	**8**	<5	<1	June 8	122937
9.991	**-45**	**0**	**4**	<2	<1	June 8	133857
9.991	-35	5	<2	**3**	<1	June 8	133857
9.991	-25	15	<3	**4**	<1	June 8	134803
2.833	**-45**	**0**	**4**	***3***	<1	June 8	162525
2.833	-35	5	<3	**3**	<1	June 8	162525
2.833	-25	15	<3	**3**	<1	June 8	160156

Legend for each column	**Behind wind farm** Not behind wind farm	**Dominant effect** ***Possibly contributing effect*** Not dominant effect	**Spiky effect**		

Table 4.4 Assessment of phase variations as function of angle and frequency, encoded by font weighting (see legend at bottom of table).

- Terrain signature (identified as all signatures not supported by wind farm scattering model while supported by general terrain scattering models) is typically of the order of $3^\circ \pm 2^\circ$, at the short range configuration it increases to $10^\circ \pm 5^\circ$. These values show no significant variation with frequency for the given locations at the same range. For backscatter locations at short range the terrain variation increases to $10^\circ \pm 5^\circ$.
- The "wind farm rotor signature" is large, up to $150^\circ \pm 50^\circ$ degrees peak behind and close to wind farm. This is ONLY observed at a single frequency 2.212 MHz and at some locations. Further investigations are needed to clarify the origin of this effect.

The current measurements indicate that, at the studied frequencies, wind farm fingerprint (phenomenon 1) is dominant over terrain signature (phenomenon 2) only at locations behind the wind farm. This applies to all frequencies studied.

4.16 Advice for future similar campaigns

Results from the measurement campaign presented above suggest that scattering from wind farms may have strong influence at direction finding sites, but are not sufficiently comprehensive to allow firm conclusions to be drawn (it might also be possible to explain the observed phase fluctuations by other phenomena). To be able to conclude more firmly, the following types of similar measurement campaigns might be performed:

1. Perform a new and more extensive measurement campaign at Smøla, in order to verify, understand better, and quantify the observed effects. Including more accurate amplitude measurements would allow discrimination between shadowing and scattering effects. More measurements with the transmitter near the position and frequency where extreme phase fluctuations were observed, and with the receiver in different positions, would strengthen or weaken the evidence that the extreme fluctuations are related to blade rotation.
2. Perform measurements in a location geographically and topographically similar to Smøla, but without any wind farm. The receiver antennas should be close to shore as well as far from shore, to find out what type of phase difference fluctuations can be expected from the ground-sea reflection as well as from other scattering effects.
3. If a new large wind farm is going to be installed, one could make measurements with exactly the same geometry before and after the wind turbines are installed. This is likely to provide clear evidence of any scattering from wind farms, but would obviously be a long-term project.

For future similar campaigns, the following advice (lessons learnt) should be kept in mind to ensure collection of high-quality measurement data:

1. The receiver site should be in a topographically smooth area, several wavelengths from shore. The site should also be easily accessible by car.

2. One should consider utilizing ground planes (radials) for the vertical receiver antennas, to minimize the influence of local ground conditions.
3. Using two interferometers at 90 degrees angle (a total of four antennas) would give good sensitivity in all directions.
4. Measuring continuous runs where the transmitter covers 360 degrees azimuth would probably give more easily interpretable data.
5. One should strive to find a receiver site with minimum local noise (e.g., sheep fences).
6. It would be a good idea to travel to the area prior to the campaign, with one HF receiver, to find a good receiver site with low local noise.
7. The choice of boat is a trade-off between several goals: High speed, crew endurance (at least, a wind screen would be advisable), and ease of antenna mounting. If geometry allows, one could also consider mounting the transmitter on a car.
8. Ensure that the data acquisition hardware is provided with an accurate clock synchronization signal.
9. Save the received audio signals as well, as these may provide additional information.
10. Include instrumentation to measure received signal level more exactly, in order to identify any shadowing effects caused by the wind farm.
11. Ask the operator to turn off the wind farm for parts of the campaign, in order to verify whether phase fluctuations are related to blade rotation.
12. Perform measurements at more frequencies, e.g., around 5 MHz and around 15 MHz.

5 CONCLUSIONS

*When the transmitter-receiver path **does not** pass directly over or near the wind farm*, it can not be concluded that there is any influence of wind farms on the communication systems or direction finding systems. In all these situations it has been found that there exist natural variations due to terrain and propagation factors, but no effects were observed that can be positively attributed to wind farms. This is based on measurements and observations in one specific area only and with given limitations in equipment accuracy and number of measurements taken. In particular, the receiver antenna positions during the measurements were unfortunate, such that natural variations may have been exaggerated. As this conclusion is based on assessments at 2MHz and 10MHz where maximum influence is expected, it may also be concluded that at lower frequencies where the interaction is weakened by wavelength in the fourth power this is also the case. At frequencies higher than 10MHz these assumptions are also expected to hold up to the point where ground wave propagation is not dominant.

*When the transmitter-receiver path **does** pass directly over or near the wind farm*, the experiments have uncovered larger than expected variations for certain locations. Due to limitations in the given experimental setup it is however not possible to conclude that this is

entirely due to wind farm effects or instruments effects due to the low signal levels present. There is some theoretical evidence that absorption of the direct ray by resonant interaction of the field by the wind turbine structures could cause these effects.

The overall conclusion of this study is that specific care and consideration should be taken when wind farms are positioned near the line of sight of HF communication and direction finding services utilizing potential ground wave paths (up 50 km range over land and 500 km over sea). To quantify and confirm the observed effects, further measurements would be required.

For non-line of sight (sky wave) arrangements influences are expected to be weaker, but exact extrapolation of the results is difficult since it is unknown how much of the observed effects are attributed to scattering vs shadowing. Any observable effects for sky wave are supposed to be maximum when the transmitter is behind the wind farm, and the signal arrives at low elevation angles. If the dominant effect is shadowing, effects may only be expected when the incoming signal passes less than a wavelength above the wind farm. If the dominant effect is scattering, effects may be expected at elevation angles up to about 10 degrees (see last paragraph of Sec. 4.8). Since the incoming signal is approximately equally strong at the wind farm and the receiver, any scattering effects are expected to be weaker than for ground waves where the signal is stronger at the wind farm.

6 ACKNOWLEDGMENTS

The authors wish to extend their thanks to the following for great help during the measurement campaign at Smøla: Senior Engineer Bjørn Skeie at FFI, whose expert knowledge of instrumentation was essential in building and testing the experimental setup, and who also carried out the measurements at the receiver location at Smøla with the utmost professionalism. Thomas Aarholt and Magnar Hjelmstad, working as research assistants at NTNU, who operated the remote HF transmitter unit and GPS tracking unit with great care and attention to detail on land and in the harsh conditions on the high speed boat. Magne Lillehaug at Smøla Havfiskesenter, who provided and drove the boat. Statkraft AS, in particular Jan Hågå who took care of practical arrangements and Geir Wang who provided data on rotation rates.

Thanks are also extended to Knut Inge Hvidsten for laying a good foundation for this work in 2005, while he was still at FFI.

References

(1) Boman T and Petterson L (2000): Direction Finding Error Due to Scattering from Wind Mills, Analysis and Computations. Scientific report FOA-R–00-01522-616–SE, FOI, Linköping, Sweden.

(2) Gjessing D T (1978): *Remote Surveillance by Electromagnetic Waves*. CRC Press Inc.

(3) Goodman J M (1992): *HF Communications. Science and Technology*. Van Nostrand Reinhold, New York, NY, USA.

(4) Hvidsten K I (2005): A Comparison Between Measurements and Predictions of HF Groundwave Propagation. FFI/RAPPORT 2005/01703, FFI, Kjeller, Norway.

(5) (1992): Rec. ITU-R P.368-7: Ground-Wave Propagation Curves for Frequencies Between 10 kHz and 30 MHz.

(6) Norton K A (1936): The Propagation of Radio Waves over the Surface of the Earth and in the Upper Atmosphere. Part I: Ground-Wave Propagation from Short Antennas. *Proc. of the IRE*, 24(10):1367–1387.

(7) Norton K A (1937): The Propagation of Radio Waves over the Surface of the Earth and in the Upper Atmosphere. Part II: The Propagation from Vertical, Horizontal, and Loop Antennas over a Flat Earth of Finite Conductivity. *Proc. of the IRE*, 25(9):1203–1236.

(8) Sengupta D L and Senior T B A (1979): Wind Turbine Generator Interference to Electromagnetic Systems. Final report 014438-3-F, US Department of Energy, Washington D.C., USA.

(9) Vincenty T (1975): Direct and Inverse Solutions of Geodesics on the Ellipsoid with Application of Nested Equations. *Survey Review*, XXII(176):88–93.

(10) Wait J R and Spies K P (1964): Propagation of Radio Waves Past a Coast Line with a Gradual Change of Surface Impedance. *IEEE Trans. Antennas and Propagation*, 12(5):570–575.